CENTRE FOR ORE DEPOSIT AND EXPLORATION STUDIES

# STRUCTURE AND MINERALISATION OF WESTERN TASMANIA

**AMIRA Project P.291A**
**Second report**
October 1994


UNIVERSITY OF TASMANIA

# Contents





# Executive Summary

**Ron Berry**

*Centre for Ore Deposit and Exploration Studies*

The last report for project P291A, Faulting and mineralisation in western Tasmania, was in May 1994. Since then the project has concentrated on detailed laboratory analysis from the last field season. Two sections have been active. The S isotope study (Davidson G & Kitto PA)has concentrated on the northern margin of Rosebery and is starting to tackle the problem of what the signature of hydrothermal circulation is in the CVC.

Sixty four sulfur isotope analyses were obtained from footwall rocks at the north end of the Rosebery hydrothermal system, using a laser ablation microprobe at the University of Tasmania. Results to date indicate that the Cambrian footwall pyrite within 1 km of B-lens has the same isotopic values as B-lens and its underlying footwall pyrite ($\delta^{34}S$ = 7.3–17.3‰, mean =11.5‰), but beyond this increases distinctly to $\delta^{34}S$ =11.8–20.2‰, with a mean of 15.1‰. Post-cleavage pyrite ranged from 1.1‰ to 3.8‰ (n=4). Black slate pyrite was divided for sampling purposes into vein and disseminated pyrite, which have the same wide isotopic range ($\delta^{34}S$= 4.6–19.2‰), although in the two samples where both types could be analysed together, vein pyrite was up to 4‰ lighter.

The increase in $\delta^{34}S$ values of footwall pyrite at Rosebery indicates that the margins of this Cambrian hydrothermal system contained high concentrations of seawater sulfate-derived sulfur. This sulfur was entrained by shallow convection at the periphery of the main up-flow limb of a deep convective cell below Rosebery. The increase in $\delta^{34}S$ values occurs further from ore, and is less pronounced, than at Hellyer. These differences are attributed to the original highly porous character of the Rosebery footwall, and leads to the general conclusion that fluid flow in the felsic breccias (which typify much of the Mount Read Volcanic Belt) must have been more diffuse than in coherent lava sequences such as the Que-Hellyer belt.

The other major activity since May has been the analysis of the stratigraphic correlation within the Mt Read volcanics, aimed at the establishment of a basin geometry. The Mt Read Volcanics have been subdivided into three depositional cycles each with a distinct basin geometry and history. This subdivision has been substantially revised from the version available in the May report with input available from a number of additional sources. Samples of sandstones have been collect from each of these cycles. Cycle 2, sandstones are recognisable from the very large component of Fe oxides, including ilmenite and magnetite. The cycle 3 sandstones have much less Fe oxide and the major external contribution to the heavy minerals is chromite and rounded zircon. These are most abundant in the Animal Creek Greywacke. The heavy mineral suites have potential to aid correlation within the stratigraphy.

Research by CODES students outside the AMIRA project is producing important results relevant to the project. A summary of two of these



studies is included here as the work is not yet generally available, and is important to the arguments in this report.

# Lithostratigraphic correlation in the Dundas and Central Volcanic Complex: progress report 2

**R.F. Berry**

*Centre for Ore Deposit and Exploration Studies*

## Abstract

The Mt Read Volcanics have been subdivided into three depositional cycles each with a distinct basin geometry and history. This sub-division has been substantiall revised from the version available in the last report with input available from a number of additional sources. Samples of sandstones have been collect from each of these cycles. Cycle 2, sandstones a recognisble from the very large component of Fe oxides, including ilmenite and magnetite. The cycle 3 sandstones have much less Fe oxide and the major external contribution to the heavy minerals is chromite and rounded zircon. These are most abundant in the Animal Creek Greywacke. The heavy mineral suites have some potential to aid correlation of the stratigraphy.

## Introduction

A major aim of the combined ARC-AMIRA project is to find new methods to enhance lithostratigraphic correlation within the Dundas Group and between the sections of the Mt Read Volcanics generally. This includes attempting to check existing lithostratigraphic sections. The major rationale of this work is to tighten up the structural interpretations in the existing regional sections and to provide a framework for basin analysis.

Several lines of evidence have already been put forward for correlation. Biostratigraphy has been used as a basis for correlation (e.g. Jago 1979, Pemberton & Corbett 1992). Lithostratigraphic correlation has been made in the northern section of the Mt Read Belt (Pemberton & Corbett 1992, McKibben 1993). McPhie & Allen (1992) suggested alternative correlations based on volcanic facies analysis in the Hellyer to Hercules section. Major new work on the Tyndall Group (White and McPhie at CODES, see review in this report) has put the stratigraphic correlation in the southern section on a firmer footing. Scott Halley provided detailed feedback on the first version of this report which has been used to produce improved summaries of the stratigraphy which are provided below. Dave Selley has provided improvements in the stratigraphy for the Dundas Group in the Dundas field. A summary of his data is included in this volume.

## Stratigraphic Correlation

The threefold classification of the Mount Read volcanics has been improved as a result of this information. The latest version is included here as a basis for continuing studies on the basin geometry and evolution.



CYCLE 1 Denison Group biostratigraphic correlates

All the units which are Idamean or younger.

CYCLE 2 Tyndall cycle of deposition

upper Boomerangian/Mindallyian

In the previous version the base of this unit was taken at the facies marker unit of McPhie & Allen (1992) but arising out of discussions with Scott Halley and Matt White, I have moved the boundary up to the base of the distinctive magnetite bearing sequence which forms the basal Comstock Tuff. This unit has now been recognised from Lynchford to the Dial Range. Dave Selley argues that much of the "upper Brewery Junction Formation" belongs in this cycle. He also suggests the Red Lead Conglomerate is probably much younger than previously proposed and correlates with the Fernfields conglomerate.

CYCLE 3 Yolande cycle of deposition

Undillian/lower Boomerangian (predate granite intrusions)

The version used here includes everything under the Tyndall Group. There is major unconformity and granite intrusion between cycle 3 and cycle 2. The volcaniclastic facies of McPhie and Allen forms a tie through the centre of the stratigraphy. This emphasises the difference in stratigraphic position between CVC at Mt Lyell and the CVC at Mt Block/Mt Black/Mt Read. The correlation has been drawn as if the CVC has an older base than the rest of the stratigraphy. There is no evidence at this stage to support such a conclusion. The greater thickness in the Rosebery-Pinnacles-Hellyer area may reflect rates of accumulation rather than longer time frames.

## Provenance and Stratigraphic Correlation

Heavy minerals are a good test of the provenance of sandstones. They potentially survive minor alteration and deformation. The phases are characteristic of their source. The distribution should say something about the basin architecture. In addition if certain sources only become available during the history of the belt a separation of the stratigraphy should be possible. For example the existing problem with the definition of the Tyndall Group. At present some granitic clasts are required to recognise this group as distinct from the Eastern Quartz-phyric sequence. Sandstones from all cycles and scattered across the belt have been included in the initial study.

Forty samples have been collected and crushed gently as recommended by Henningsen (1967). The fine sand fraction from these rocks were extracted by sieving, washed and then separated by heavy liquids.

The heavy mineral separations have been running over the last six months. Twenty heavy mineral suites have been mounted on polished thin sections. Of these a detailed point count has been carried out on a dozen sample and four have been checked by microprobe analysis. This is taking longer than expected. It seems likely that whole rock analyses would be a much more efficient process and in most cases produce sufficient information on the provenance of the sandstones. The following report represents an interim stage in the analysis. This will continue until the first 40 samples are complete before a final decision to change to whole rock analyses is made.

The heavy mineral contents are summarised in Table 1. The results of this analysis are shown below.

1. The Tyndall Group is distinguished by high Fe oxide contents. these include magnetite, hematite and ilmenite plus the oxidised equivalents. The Tyndall group samples also

contain $TiO_2$, mostly as anatase where they are weathered, so that these rocks overall have FeO ≈ $TiO_2$. The total heavy mineral suite is high, about 1% of sample. The rocks have low zircon and tourmaline, possibly due to dilution effects. On this basis the sample (94/20, ?Jukes Conglomerate) from Murchison Gorge, 7 m below the Owen Conglomerate, has typical Tyndall Group heavy minerals with a very high ilmenite content. The high oxide content appears to be typical of all of the Tyndall Group and is not limited to the lower andesitic part.

2. The Animal Creek Greywacke has a distinctive association of high chromite, high $TiO_2$, very low Fe oxides, high zircon and tourmaline but low apatite content. The Animal Creek Greywacke is the only suite considered in which well rounded zircons forming a substantial part of the total zircon suite.

The Farrell Slates at the Mackintosh Dam have a heavy mineral suite which is very similar to the Animal Creek Greywacke supporting correlation of these two units. Chromite is common as are rounded zircons with apatite and tourmaline also significant. They have very low Fe oxides.

The sandstone sample from the Strahan Highway (94/38) has substantial chromite, high $TiO_2$, low Fe oxides but little zircon and tourmaline. The point counting is incomplete and a more detailed look at the heavy minerals in this rock will be carried out to test correlation with the Animal Creek greywacke.

The two sample from the Boco Road (94/3, 94/8) which are from just above the Animal Creek Greywacke are very different from the Animal Creek Greywacke with low chromite, low $TiO_2$ (for 94/3) and high Fe oxides. Both contain substantial pyrite which may be effecting the level of Fe oxide by contributing to goethite.

The Stitt Quartzite at Rosebery is zircon rich with high Fe oxides and low $TiO_2$. It does have a high component of rounded zircon. This looks quite different from Animal Creek Formation and similar to the Boco Road samples. The Stitt "correlate" on the Boco Road (94/4) has high apatite and tourmaline, and no chromite. This is consistent with the present interpretation.

Two samples of Yolande River Group were analysed. One of these was a volcaniclastic from the Yolande River. This sample was entirely composed of euhedral zircon. No external component was recognised in this rock. A sample of micaceous sandstone from further west was dominated by pyrite and this dilution makes the statistics poor. However, there was no evidence for a chromite component or high $TiO_2$. However there is a high component of chlorite. Neither sample show any evidence for a source from outside the Mt Read volcanics, but more work needs to be done on 94/32 to overcome the high dilution effects of the pyrite.

The sample from Merton road was pyritic and weathered so it was difficult to get a reasonable signature from this rock. The lack of chromite and general similar abundance of zircon and tourmaline supports correlation with the Yolande River Group. A larger sample of heavy minerals needs to be counted.

The Higgins Creek sample are biostratigraphical correlates of the Newton Creek Sandstone (Denison Cycle). They were both slightly weathered and this has shown in the heavy mineral suite. Both samples have Fe oxides dominant over $TiO_2$. Chromite is a minor component. The presence of ilmenite and chromite shows some similarity of source with upper Tyndall Group.



## Minerals

At this stage we have collected 150 mineral analyses from four samples. This is a very early stage in the analysis.

### Apatite

All apatites show fractured or euhedral shapes. No rounded apatites were recognised. The compositions (Table 2) are all F rich suggesting a magmatic origin, and combined with the textures, a proximal source from local magmatic activity is proposed. There is more apatite in the younger sandstones.

### Zircon

Zircons have been found in most rocks. There is very little variation in composition (Table 3). In the sample 94/11, the high Y contents are all in rounded grains but this does not yet seem to be holding up through all the samples. No other variations were detected.

### Tourmaline

Tourmalines are largely euhedral or broken. No evidence a was noted for rounded tourmaline. Some tourmalines have visible zoning in colour but this has not been investigated in detail. The compositions range in Mg#, with MgO varying from 5.8–11.3% but other elements are not very variable (Table 4).

### Magnetite

Magnetites are all heavily altered with hematite rims and replacement In many rocks there is only a few flecks of magnetite left. After coating for the microprobe it is difficult to distinguish the magnetite cores from the hematite and most of the oxide analyses (Table 5) have low totals indicating that they are largely hematite. $TiO_2$ is fairly low. The presence of ilmenite exsolution lamellae in hematised magnetite suggest titano-magnetite original compositions.

### Hematite

The irregular form of hematite grains is interpreted here to indicate the hematite is not a primary detrital mineral but replaces the magnetite and possibly ilmenite.

### Pyrite

Pyrite is a common heavy mineral. Most of the pyrite is euhedral but a minor proportion is in framboids.

One sample contained chalcopyrite and another was rich in sphalerite.

### Ilmenite

Ilmenite grains are rounded and are detrital. They are weathered with alteration to $TiO_2$. The analyses so far are all too low in $TiO_2$ for ilmenite suggesting there is extensive hematisation of the ilmenites.

### Rutile, anatase

$TiO_2$ is a common component in most rocks. Much of this especially in the Tyndall Group, is the result of weathering ilmenite and magnetite. In some samples, rutile is apparently a primary detrital phase. The Animal Creek Greywacke is the best example of this form of the $TiO_2$.

### Garnet

Surprisingly garnet has not been recognised as major contributor to the heavy mineral suite. So far only two grains have been found (in sample 94/38, Table 6). These garnets have high MgO and low CaO. The second garnet is on the margin of the range of garnets from Nye Bay. The other garnet is unusually high in MgO for this CaO content and no Tasmanian source is known. This composition suggests a granulite facies source area.

## References

Henningsen D 1967. Crushing of sedimentary rock samples and its effect on shape and number of heavy minerals. Sedimentology 8, 253-255.

Jago J B 1979. Tasmanian Cambrian biostratigraphy — a preliminary report. J Geol. Soc. Aust. 26, 223-230.

McKibben J A J 1993. The geology and geochemistry of the North Pinnacles Ridge, western Tasmania. BSc Hons. thesis (unpubl.).

McPhie J & Allen R L 1992. Facies architecture of mineralised submarine volcanic sequences: Cambrian Mount Read volcanics, western Tasmania. Econ. Geol. 87, 587-596.

Pemberton J & Corbett K D 1992. Stratigraphic-facies associations and their relationship to mineralisation in the Mt Read Volcanics. Bull. geol Surv. Tasm. 70, 167-176.



*Fig. 1 . Summary of stratigraphy in western Tasmania during the Denison Cycle*

| | | Modder River | Queenstown | Professor Range | Dundas | Rosebery Group | Huskisson Syncline | Higgins Creek | Hellyer-Mt Block | Dial Range | Smithton |
|---|---|---|---|---|---|---|---|---|---|---|---|
| 490 Ma | Datson | Qtz sandstone and conglomerate | Upper Owen Sandstone | Owen correlate | Misery Hill sandstone ◆ | | | ?Owen Comglom. at Mt Pearse | Owen Conglom-erate | Moina Sandstone | |
| | Payto | | Middle Owen Sandstone | Owen correlate | | | | | Owen Conglom. | Duncan Conglom. | |
| | Post-I-Pre-P | ◆ fine micaceous ◆ sandstone and ◆ siltstone siltstone and minor volcaniclastic sandstones | Newton Creek Sandstone ◆ | Mudstone sandstone conglomer. ◆ package ◆ of Queensberry Mine | Misery Conglomer. ◆Climie Formation | | | ◆ Siltstone and lithic wacke with channel conglomer. | | | |
| | Idamean | | Lower Owen Conglom. | | | | Sandstone and conglom. ◆ black mudstone | | | | ◆ Scopus calcareous qtz turbidites |

*Fig. 2. Summary of stratigraphy in western Tasmania during the Tyndall Cycle*

| | | Queenstown | Farrell Rivulet | Dundas | Rosebery Group | Pinnacles / Silver Hills | Hellyer-Mt Block | Tyndall range | Dial Range |
|---|---|---|---|---|---|---|---|---|---|
| 500 Ma | Mindayallan | Upper Tyndall Gp. | ◆ Upper Brewery Junction correlate<br>Farrell Riv. quartzwacke | Upper Brewery ◆ Junction (Fernflow conglomerate, Comet Slate, Fernfields comglom., Read Lead Cong.) ◆ | Salisbury Conglomerate/ Natone Volcanics | Hatfield River Sequence | upper Mt Cripps Sub-Group on Cradle Link Road | Dora Conglomerate | ◆ Radfords Creek Group |
| | upperBoo | Comstock Tuff<br>lower Comstock Tuff | | Qtz rich volcanic sst | | Magnetic Sandstone package | ◆ lower Mt Cripps Subgroup | | ◆ Radfords Creek Group |

*Fig. 3. Summary of stratigraphy in western Tasmania during the Yolande Cycle*

| | | Queenstown | Yolande River | Dundas | Huskisson Syncline | Rosebery | Pinnacles | Hellyer-Mt Block | Eastern margin | Fossey Mtn | Smithton | Dial Range |
|---|---|---|---|---|---|---|---|---|---|---|---|---|
| | Lower Boomerang | ◆ limestone member<br><br>Andesites and rhyolites at Mt Lyell<br><br>Yolande River Group | <br><br><br><br>YRG upper volcanicl. member | Razorback Conglomerate Pumiceous mass flow deposits and interbedded mudstones<br><br>◆ Hodge Slate | ◆<br><br>dominantly feldspar phyric volcanicl. of the Merton Road to Pieman River | Westcott argillite Stitt Qtzt Chamberlain Shale White Spur Formation<br><br>Rosebery host sequence | Qtz dominated sediments<br><br>Volcanic sandstones Rhyolitic lavas Black shale member | <br><br>Southwell Subgroup<br><br>◆ Que River Shale<br><br>Que Hellyer Volcanics | <br><br>Eastern quartz-phyric sequence | <br><br>◆ Native Track Tier | ◆ Christmas Hills siltstones ◆ and volcanic sandstones | |
| | Undillian | Miners Ridge Sandstone | YRG lower micaceous member | | ◆ | Rosebery footwall pumiceous volcani-clastics Mt Black volcanics | Browns Tunnel sequence<br><br>Pumiceous volcaniclastic units<br><br>CVC | Animal Creek Greywacke (upper micaceous member) Black Harry beds (lower volcaniclastic member)<br><br>CVC | Sticht Range Formation | | | ◆ Cateena Group |
| 510 Ma | Floor | | | | | Feldspathic volcaniclast. and minor andesites | CVC | CVC | | | | |

*Table 1. Summary of heavy mineral populations in sandstones from western Tasmania*

| | Animal CG | AnimalCG | AnimalCG | Farrell Sl | Farrell Sl | Strahan rd | | Boco Rd | Boco Rd | YolandeRG | YolandeR G | Stitt Qte |
|---|---|---|---|---|---|---|---|---|---|---|---|---|
| Field no | 94/11 | 94/12 | 94/14 | 94/1 | 94/2 | 94/38 | | 94/3 | 94/8 | 94/29 | 94/32 | SQ-1 |
| AMG | 811853 | 844897 | 853903 | 877833 | 874831 | 684297 | | 784850 | 793853 | 789430 | 780338 | |
| | | | | | | | | | volcani- | volcani- | micaceous | sst |
| | | | | | | | | | clastic | clastic | sst | |
| | | | | | | | | | | | | |
| pyrite | | | | 39 | 61 | | | 36 | 148 | 6 | 100 | 7 |
| magnetite | | | | | | | | 1 | 19 | | | |
| hematite | | 4 | | 1 | 4 | | | 5 | 3 | | | 29 |
| ilmenite | | 7 | | | | | | 1 | 6 | | | 4 |
| tourmaline | 32 | 18 | 92 | 3 | 6 | | | | 2 | 1 | 2 | 8 |
| zircon(euh) | 5 | 3 | 11 | 6 | | | | 1 | | 210 | 2 | 3 |
| zircon(round) | 8 | 19 | 20 | 7 | 12 | | | | 4 | 8 | | 47 |
| apatite | 3 | 38 | 2 | 10 | 10 | 1 | | 2 | | 2 | | 4 |
| chromite | 48 | 146 | 147 | 46 | 15 | 15 | | | 4 | | | 10 |
| TiO2 | 54 | 55 | 40 | 22 | 17 | 65 | | 44 | | 1 | | 9 |
| goethite | 2 | | 27 | 2 | 3 | 1 | | 13 | | 8 | 2 | |
| chlorite | 6 | 1 | 3 | 13 | 1 | 1 | | 1 | 6 | 3 | 48 | |
| other | 3 | | 2 | 7 | 8 | 4 | | | | | 74 | |
| weight | 27.8 | 29.16 | 25.9 | | 29.11 | 23.57 | | 28.59 | 22.47 | 21.31 | 18.16 | 23.54 |
| | 0.06 | 0.03 | 0.03 | | 0.07 | 0.36 | | 0.1 | 0.03 | 0.02 | 0.09 | 0.06 |
| | | | | | | | | | | | | |
| ap/tour | 0.09 | 0.68 | 0.02 | 0.77 | 0.63 | 1.00 | | 1.00 | 0.00 | 0.67 | 0.00 | 0.33 |
| TiO2/Zr | 0.81 | 0.71 | 0.56 | 0.63 | 0.59 | 1.00 | | 0.98 | 0.00 | 0.00 | 0.00 | 0.15 |
| Chrom/zr | 0.79 | 0.87 | 0.83 | 0.78 | 0.56 | 1.00 | | 0.00 | 0.50 | 0.00 | 0.00 | 0.17 |

*Table 1. Summary of heavy mineral populations in sandstones from western Tasmania. cont.*

| | StittCorr | Merton Rd | Southwell SG | Tyndall | Tyndall | Tyndall | TynCorr | Upper Tyndall Gp | Higgins Ck | Higgins Ck | Jukes C |
|---|---|---|---|---|---|---|---|---|---|---|---|
| Field no | 94/4 | 94/23 | 94/19 | 94/31 | 94/30 | 94/36 | 94/18 | 94/17 | 94/7 | 94/5 | 94/20 |
| AMG | 768846 | 677794 | 947986 | 789378 | 790374 | 838306 | 957987 | 967987 | 761861 | 753844 | 863761 |
| | BocoRd | sst | | Lynchford | Lynchford | Jukes Rd | CMlinkrd | CM linkrd | | | |
| | | | | Tuff | sst | | | sst | | | |
| | | | | | | | | | | | |
| pyrite | 30 | 35 | 4 | | | | 1 | | | | |
| magnetite | | | 2 | 101 | | 8 | | 15 | | | |
| hematite | 1 | | 17 | 3 | 3 | 2 | 72 | 13 | 3 | 94 | 3 |
| ilmenite | | | 19 | | 2 | | 29 | 23 | | 16 | 207 |
| tourmaline | 23 | 1 | 4 | 1 | 1 | | | | | 4 | |
| zircon(euh) | 12 | 2 | 1 | 1 | 15 | 9 | | | 1 | | 6 |
| zircon(round) | 12 | | | 1 | | 1 | | 2 | 2 | | 1 |
| apatite | 21 | 7 | 10 | 2 | | | 9 | 19 | | 2 | 3 |
| chromite | | | 20 | | | | 25 | | 2 | 20 | |
| TiO2 | 61 | 10 | 10 | 60 | 265 | 59 | 4 | | 9 | 27 | 5 |
| goethite | 11 | 125 | | 7 | 15 | 152 | | 63 | 202 | 68 | 1 |
| chlorite | 17 | | 1 | 9 | | | | 57 | 1 | | |
| other | 4 | 9 | | | | | | | | | |
| weight | 25.37 | 19.59 | | 26.54 | 27.11 | 24.85 | 27.88 | 22.23 | 13.82 | 32.95 | 20.86 |
| | 0.01 | 0.04 | | 0.39 | 0.02 | 0.11 | 0.47 | 0.71 | 0.05 | 1.53 | 0.52 |
| | | | | | | | | | | | |
| ap/tour | 0.48 | 0.88 | 0.71 | 0.67 | 0.00 | | 1.00 | #VALUE! | | 0.33 | 1.00 |
| TiO2/Zr | 0.72 | 0.83 | 0.91 | 0.97 | 0.95 | 0.86 | 1.00 | 0.00 | 0.75 | 1.00 | 0.42 |
| Chrom/zr | 0.00 | 0.00 | 0.95 | 0.00 | 0.00 | 0.00 | 1.00 | 0.00 | 0.40 | 1.00 | 0.00 |

*Table 2. Summary of apatite analyses in sandstones from western Tasmania.*

| | 94/41 | | | | | | 94/38 | | | | | 94/2 | | | |
|---|---|---|---|---|---|---|---|---|---|---|---|---|---|---|---|
| SiO2 | 0.66 | 0.36 | 0.37 | 0.36 | 0.32 | | 0.47 | 0.49 | 0.01 | 0.00 | | 0.35 | 0.30 | 0.26 | 0.00 |
| CaO | 52.61 | 53.31 | 52.84 | 53.29 | 53.21 | | 54.77 | 54.94 | 55.35 | 55.53 | | 55.03 | 55.03 | 55.32 | 55.61 |
| SrO | 0.05 | 0.05 | 0.05 | 0.04 | 0.02 | | 0.06 | 0.03 | 0.28 | 0.32 | | 0.01 | 0.07 | 0.05 | 0.00 |
| FeO | 0.67 | 0.66 | 0.79 | 0.71 | 1.08 | | 0.34 | 0.73 | 0.09 | 0.04 | | 0.16 | 0.38 | 0.36 | 0.04 |
| MgO | 0.16 | 0.07 | 0.09 | 0.11 | 0.00 | | 0.19 | 0.10 | 0.00 | 0.00 | | 0.05 | 0.14 | 0.03 | 0.00 |
| P2O5 | 42.92 | 42.73 | 43.04 | 42.93 | 42.84 | | 40.02 | 39.81 | 41.08 | 41.34 | | 40.75 | 40.31 | 40.59 | 41.22 |
| F | 4.31 | 4.31 | 4.54 | 4.01 | 4.11 | | 4.17 | 4.59 | 3.62 | 4.19 | | 5.17 | 4.88 | 4.06 | 5.39 |
| Cl | 0.43 | 0.42 | 0.25 | 0.22 | 0.19 | | 0.74 | 0.59 | 0.01 | 0.01 | | 0.02 | 0.02 | 0.02 | 0.01 |

*Table 3. Summary of zircon analyses in sandstones from western Tasmania.*

| | 94/11 | | | | | | | | | 94/41 | | 94/38 |
|---|---|---|---|---|---|---|---|---|---|---|---|---|
| SiO2 | 29.81 | 29.66 | 29.37 | 30.00 | 30.37 | 30.19 | 29.75 | 30.27 | | 30.71 | | 31.22 |
| Y2O3 | 0.30 | 0.00 | 0.29 | 0.04 | 0.00 | 0.23 | 0.00 | 0.05 | | 0.42 | | 0.03 |
| ZrO2 | 63.77 | 63.05 | 60.82 | 62.06 | 63.86 | 63.61 | 59.73 | 62.13 | | 63.27 | | 66.21 |
| La2O3 | 0.01 | 0.00 | 0.00 | 0.00 | 0.00 | 0.00 | 0.01 | 0.01 | | 0.00 | | 0.02 |
| HfO2 | 1.06 | 1.37 | 1.40 | 1.46 | 1.58 | 1.25 | 1.66 | 1.95 | | 1.34 | | 1.46 |
| ThO2 | 0.00 | 0.00 | 0.05 | 0.10 | 0.00 | 0.17 | 0.01 | 0.06 | | 0.01 | | 0.00 |

| | 94/38 | | | | 94/2 | | | | |
|---|---|---|---|---|---|---|---|---|---|
| SiO2 | 27.87 | 31.04 | 31.19 | | 31.17 | 31.00 | 31.39 | 31.16 | 31.58 |
| Y2O3 | 0.70 | 0.06 | 0.03 | | 0.00 | 0.08 | 0.00 | 0.09 | 0.00 |
| ZrO2 | 62.90 | 64.56 | 64.30 | | 65.48 | 65.68 | 64.65 | 65.13 | 65.41 |
| La2O3 | 0.00 | 0.00 | 0.01 | | 0.00 | 0.00 | 0.00 | 0.00 | 0.00 |
| HfO2 | 1.33 | 1.45 | 1.36 | | 1.59 | 1.62 | 1.43 | 1.64 | 1.23 |
| ThO2 | 0.08 | 0.15 | 0.00 | | 0.05 | 0.05 | 0.00 | 0.00 | 0.01 |

*Table 4. Summary of tourmaline analyses in sandstones from western Tasmania.*

| | 94/11 | | | | | | | | | |
|---|---|---|---|---|---|---|---|---|---|---|
| SiO2 | 34.67 | 36.42 | 35.38 | 35.26 | 39.09 | 34.02 | 34.94 | 35.26 | 34.18 | 34.54 |
| Al2O3 | 29.28 | 31.87 | 32.11 | 32.87 | 28.07 | 31.77 | 32.01 | 30.99 | 31.72 | 30.94 |
| TiO2 | 0.55 | 0.45 | 0.96 | 0.33 | 0.48 | 0.44 | 0.49 | 0.66 | 0.54 | 0.76 |
| FeO | 9.16 | 7.20 | 8.08 | 6.41 | 6.44 | 9.44 | 9.27 | 7.18 | 10.27 | 10.18 |
| MnO | 0.10 | 0.00 | 0.00 | 0.05 | 0.00 | 0.14 | 0.18 | 0.00 | 0.07 | 0.06 |
| MgO | 7.64 | 5.93 | 5.76 | 6.44 | 8.77 | 5.85 | 5.99 | 7.94 | 4.79 | 5.07 |
| CaO | 0.79 | 0.11 | 0.07 | 0.21 | 0.19 | 0.76 | 0.63 | 0.29 | 0.68 | 0.07 |
| K2O | 0.02 | 0.03 | 0.01 | 0.01 | 0.02 | 0.06 | 0.06 | 0.01 | 0.05 | 0.02 |
| Na2O | 2.27 | 1.99 | 2.09 | 1.92 | 2.63 | 1.94 | 2.06 | 2.30 | 1.94 | 2.28 |
| F | 0.49 | 0.34 | 0.14 | 0.37 | 0.15 | 0.35 | 0.22 | 0.36 | 0.06 | 0.50 |

| | | | | | | | | 94/2 | | | |
|---|---|---|---|---|---|---|---|---|---|---|---|
| SiO2 | 36.23 | 36.51 | 35.61 | 34.88 | 35.05 | 34.73 | | 36.44 | 36.26 | 35.54 | 35.89 |
| Al2O3 | 30.72 | 32.06 | 31.82 | 32.88 | 32.15 | 29.97 | | 31.11 | 30.88 | 31.34 | 31.55 |
| TiO2 | 0.46 | 0.24 | 0.18 | 0.43 | 0.95 | 0.88 | | 0.50 | 0.51 | 0.93 | 0.76 |
| FeO | 3.69 | 1.08 | 4.34 | 5.51 | 8.59 | 10.16 | | 7.41 | 7.07 | 9.75 | 9.16 |
| MnO | 0.00 | 0.00 | 0.00 | 0.00 | 0.01 | 0.00 | | 0.00 | 0.00 | 0.00 | 0.04 |
| MgO | 10.33 | 11.32 | 9.31 | 7.89 | 6.08 | 6.57 | | 7.81 | 8.10 | 5.90 | 6.21 |
| CaO | 0.19 | 0.26 | 0.98 | 1.26 | 0.25 | 0.03 | | 0.21 | 0.70 | 0.29 | 0.40 |
| K2O | 0.03 | 0.01 | 0.02 | 0.07 | 0.01 | 0.01 | | 0.00 | 0.02 | 0.02 | 0.01 |
| Na2O | 2.72 | 2.76 | 1.74 | 1.90 | 2.42 | 2.44 | | 2.60 | 2.30 | 2.44 | 2.32 |
| F | 0.57 | 0.77 | 0.53 | 0.16 | 0.29 | 0.12 | | 0.12 | 0.15 | 0.25 | 0.26 |

| | | |
|---|---|---|
| SiO2 | 36.41 | 36.64 |
| Al2O3 | 30.08 | 30.63 |
| TiO2 | 0.24 | 0.23 |
| FeO | 8.48 | 7.43 |
| MnO | 0.02 | 0.00 |
| MgO | 8.23 | 8.35 |
| CaO | 0.57 | 0.47 |
| K2O | 0.02 | 0.03 |
| Na2O | 2.36 | 2.41 |
| F | 0.28 | 0.34 |



*Table 5. Summary of oxide analyses in sandstones from western Tasmania.*

| | 94/11 | | | | | | | | 94/38 | | | | | | | | | | |
|---|---|---|---|---|---|---|---|---|---|---|---|---|---|---|---|---|---|---|---|
| Tot Fe2O3 | 0.28 | 0.14 | 0.46 | 0.23 | 0.12 | 0.49 | 0.48 | 0.26 | 5.66 | 3.37 | 3.07 | 2.74 | 2.51 | 3.67 | 8.66 | 2.87 | 2.29 | 0.34 | 0.07 |
| TiO2 | 90.22 | 94.78 | 95.39 | 95.08 | 95.63 | 88.94 | 93.87 | 95.36 | 71.60 | 81.01 | 82.04 | 81.09 | 81.87 | 80.85 | 67.21 | 80.91 | 84.08 | 93.99 | 93.60 |
| Cr2O3 | 0.00 | 0.16 | 0.02 | 0.07 | 0.11 | 0.01 | 0.02 | 0.18 | 0.08 | 0.08 | 0.08 | 0.09 | 0.11 | 0.12 | 0.03 | 0.09 | 0.14 | 0.05 | 0.01 |
| Al2O3 | 1.42 | 0.00 | 0.00 | 0.00 | 0.00 | 1.62 | 0.00 | 0.00 | 5.57 | 3.07 | 2.87 | 3.07 | 3.10 | 3.17 | 5.58 | 3.48 | 2.19 | 0.09 | 0.00 |
| MnO | 0.00 | 0.00 | 0.00 | 0.00 | 0.00 | 0.00 | 0.02 | 0.00 | 0.01 | 0.00 | 0.00 | 0.00 | 0.00 | 0.00 | 0.00 | 0.00 | 0.00 | 0.00 | 0.00 |
| MgO | 0.26 | 0.00 | 0.00 | 0.00 | 0.00 | 0.22 | 0.00 | 0.00 | 1.72 | 1.21 | 0.53 | 0.98 | 1.07 | 1.32 | 3.67 | 1.14 | 0.91 | 0.00 | 0.00 |
| ZnO | 0.00 | 0.03 | 0.00 | 0.00 | 0.00 | 0.10 | 0.07 | 0.00 | 0.00 | 0.04 | 0.00 | 0.03 | 0.00 | 0.00 | 0.01 | 0.00 | 0.05 | 0.11 | 0.00 |

| | 94/2 | | | | | | 94/41 | | | | | | | | | | | | |
|---|---|---|---|---|---|---|---|---|---|---|---|---|---|---|---|---|---|---|---|
| Tot Fe2O3 | 0.15 | 0.19 | 0.47 | 0.31 | 0.14 | | 87.14 | 86.07 | 84.07 | 80.78 | 83.16 | 80.13 | 81.12 | 75.48 | 59.67 | 66.82 | 65.84 | 65.35 | 65.36 |
| TiO2 | 90.15 | 92.88 | 92.06 | 93.11 | 93.89 | | 1.45 | 3.19 | 3.69 | 5.62 | 6.43 | 6.46 | 6.79 | 11.43 | 18.58 | 23.28 | 23.69 | 24.17 | 26.54 |
| Cr2O3 | 0.04 | 0.06 | 0.02 | 0.03 | 0.06 | | 0.00 | 0.60 | 0.57 | 0.02 | 0.40 | 0.09 | 0.06 | 0.10 | 0.00 | 0.15 | 0.11 | 0.14 | 0.04 |
| Al2O3 | 0.00 | 0.00 | 0.00 | 0.00 | 0.00 | | 0.88 | 0.56 | 0.60 | 0.37 | 0.34 | 2.12 | 1.37 | 2.71 | 8.76 | 0.26 | 0.07 | 0.32 | 0.00 |
| MnO | 0.00 | 0.01 | 0.02 | 0.00 | 0.02 | | 0.22 | 0.11 | 0.15 | 1.24 | 0.07 | 0.13 | 0.08 | 0.06 | 0.03 | 0.08 | 0.00 | 0.00 | 0.02 |
| MgO | 0.00 | 0.00 | 0.00 | 0.00 | 0.01 | | 0.05 | 0.12 | 0.13 | 2.11 | 0.17 | 1.05 | 0.45 | 1.10 | 1.22 | 0.14 | 0.07 | 0.18 | 0.00 |
| ZnO | 0.02 | 0.03 | 0.00 | 0.00 | 0.00 | | 0.07 | 0.01 | 0.00 | 0.07 | 0.08 | 0.02 | 0.06 | 0.03 | 0.04 | 0.00 | 0.05 | 0.01 | 0.00 |

| | | | | | | | | | | | 94/38 | | | | | | | | |
|---|---|---|---|---|---|---|---|---|---|---|---|---|---|---|---|---|---|---|---|
| Tot Fe2O3 | 64.56 | 62.49 | 57.46 | 54.29 | 55.19 | 54.76 | 54.66 | 55.52 | 54.59 | 50.74 | 92.78 | 91.16 | 93.30 | 92.50 | 92.69 | 92.92 | 93.90 | 93.20 | 92.64 |
| TiO2 | 27.71 | 28.45 | 33.73 | 36.12 | 36.66 | 36.99 | 37.02 | 37.03 | 37.42 | 38.88 | 0.33 | 0.57 | 0.26 | 0.47 | 0.86 | 0.29 | 0.19 | 0.20 | 0.17 |
| Cr2O3 | 0.03 | 0.13 | 0.06 | 0.12 | 0.00 | 0.03 | 0.04 | 0.01 | 0.00 | 0.04 | 0.16 | 0.16 | 0.08 | 0.09 | 0.17 | 0.13 | 0.14 | 0.14 | 0.16 |
| Al2O3 | 0.01 | 0.19 | 0.00 | 0.25 | 0.14 | 0.00 | 0.27 | 0.00 | 0.17 | 0.53 | 0.09 | 0.04 | 0.02 | 0.05 | 0.17 | 0.06 | 0.04 | 0.39 | 0.07 |
| MnO | 0.00 | 0.00 | 0.00 | 0.08 | 0.00 | 0.03 | 0.02 | 0.04 | 0.09 | 0.00 | 0.17 | 0.27 | 0.05 | 0.07 | 0.49 | 0.13 | 0.07 | 0.10 | 0.08 |
| MgO | 0.01 | 0.20 | 0.04 | 0.18 | 0.09 | 0.01 | 0.00 | 0.01 | 0.01 | 0.06 | 0.00 | 0.02 | 0.01 | 0.01 | 0.00 | 0.01 | 0.00 | 0.00 | 0.00 |
| ZnO | 0.00 | 0.03 | 0.00 | 0.00 | 0.03 | 0.02 | 0.06 | 0.00 | 0.04 | 0.02 | 0.06 | 0.06 | 0.00 | 0.00 | 0.00 | 0.00 | 0.03 | 0.15 | 0.00 |

| | | | | 94/2 | | | | | | | | | | | |
|---|---|---|---|---|---|---|---|---|---|---|---|---|---|---|---|
| Tot Fe2O3 | 92.67 | 91.71 | 92.66 | 93.29 | 92.95 | 86.99 | 89.09 | 91.06 | 92.16 | 90.29 | 89.93 | 93.10 | 90.28 | 88.20 | 91.35 |
| TiO2 | 0.13 | 0.21 | 0.49 | 0.02 | 0.05 | 0.24 | 0.08 | 0.06 | 0.05 | 0.10 | 0.11 | 0.01 | 0.11 | 0.13 | 0.10 |
| Cr2O3 | 0.12 | 0.11 | 0.12 | 0.00 | 0.00 | 0.02 | 0.01 | 0.02 | 0.00 | 0.01 | 0.00 | 0.02 | 0.01 | 0.00 | 0.00 |
| Al2O3 | 0.02 | 0.05 | 0.05 | 0.07 | 0.06 | 1.60 | 0.64 | 0.11 | 0.14 | 0.58 | 0.52 | 0.03 | 0.47 | 0.79 | 0.60 |
| MnO | 0.06 | 0.13 | 0.00 | 0.05 | 0.06 | 0.09 | 0.00 | 0.04 | 0.05 | 0.05 | 0.10 | 0.06 | 0.04 | 0.00 | 0.01 |
| MgO | 0.00 | 0.00 | 0.00 | 0.00 | 0.00 | 0.09 | 0.03 | 0.07 | 0.03 | 0.01 | 0.02 | 0.00 | 0.01 | 0.04 | 0.04 |
| ZnO | 0.03 | 0.04 | 0.00 | 0.05 | 0.01 | 0.00 | 0.00 | 0.00 | 0.04 | 0.00 | 0.00 | 0.04 | 0.00 | 0.03 | 0.00 |

*Table 6. Summary of garnet analyses in sandstones from western Tasmania.*

| | 94/38 | 94/38 |
|---|---|---|
| SiO2 | 38.37 | 37.35 |
| Al2O3 | 21.70 | 21.24 |
| Cr2O3 | 0.13 | 0.23 |
| FeO | 28.12 | 30.26 |
| MnO | 0.44 | 1.07 |
| MgO | 9.43 | 6.25 |
| CaO | 1.60 | 3.26 |



# Progress Report : Detecting Cambrian structures in the Mt Read Volcanic Belt using sulfur isotopes — case study: Rosebery

**Garry J. Davidson & Paul Kitto**

*Centre for Ore Deposit and Exploration Studies*

## Abstract

Sixty four sulfur isotope analyses were obtained from footwall rocks at the north end of the Rosebery hydrothermal system, using a laser ablation microprobe at the University of Tasmania. Most of the samples were systematically distributed in the top 100 m of the footwall sequence, at intervals of 0, 968 and 1781 horizontal metres from B-lens. Pyrites from the host-sequence epiclastics and black slates were also analysed. The morphology of pyrite in all of these rocks was studied petrographically, to determine if links exist between morphology and isotopic composition. Cambrian pyrite has experienced significant metamorphism and deformation, resulting in recrystallised sub- to euhedral habits. Some minor Devonian? pyrite was identified on the basis of its anhedral irregular habit (indicating a post-cleavage emplacement), and its association with pyrrhotite and carbonate. Results to date indicate that the Cambrian footwall pyrite within 1 km of B-lens has the same isotopic values as B-lens and its underlying footwall pyrite ($\delta^{34}S$ = 7.3–17.3‰, mean = 11.5‰), but beyond this increases distinctly to $\delta^{34}S$ =11.8–20.2‰, with a mean of 15.1‰. Devonian? pyrite ranged from 1.1‰ to 3.8‰ (n = 4). Black slate pyrite was divided for sampling purposes into vein and disseminated pyrite, which have the same wide isotopic range ($\delta^{34}S$= 4.6–19.2‰), although in the two samples where both types could be analysed together, vein pyrite was up to 4‰ lighter.

The increase in $\delta^{34}S$ values of footwall pyrite at Rosebery indicates that the margins of this Cambrian hydrothermal system contained high concentrations of seawater sulfate-derived sulfur. This sulfur was entrained by shallow convection at the periphery of the main upflow limb of a deep convective cell below Rosebery. The increase in $\delta^{34}S$ values occurs further from ore, and is less pronounced, than at Hellyer. These differences are attributed to the original highly porous character of the Rosebery footwall, and leads to the general conclusion that fluid flow in the felsic breccias (which typify much of the Mount Read Volcanic Belt) must have been more diffuse than in coherent lava sequences such as the Que-Hellyer belt.

Following this work, sulfur isotope values can be used to identify Cambrian structures which have experienced medium temperature (~200°C) seawater circulation. At these temperatures seawater sulfate will be at least partially reduced, and new pyrite significantly heavier than ambient igneous pyrite in volcanic rocks (probably $\delta^{34}S$ = $4 \pm 4$‰).

## Introduction

A review of sulfur isotope behaviour in altered volcanic rocks was presented in Davidson & Kitto (1994). The conclusions of the review with respect



to the detection of Cambrian structures were that

(1) Cambrian fluids that had been heated to 300–400° C would produce sulfur in the range 4–15‰, derived from a combination of leached host-volcanic sulfur and reduced seawater sulfate. Sulfides with this isotopic value, and associated quartz-sericite alteration, are a strong indicator that a particular structure was a fluid conduit for deeply sourced Cambrian hydrothermal fluids. These structures are not a priority of this study, because they are likely to have been already recognised given the intense exploration activity in the Mt Read Volcanic Belt.

(2) Cambrian structures associated with shallow convection— either on the peripheries of major circulation cells, or as the focus of smaller hydrothermal systems — might well be isotopically recognisable as zones of heavier sulfur, approaching the seawater sulfate value (Cambrian: $\delta^{34}S$ = 30‰). At these sites it is suggested that sulfur derived from the partial reduction of seawater sulfate dominated over the rock-leached sulfur component in the fluid. The best evidence for this has come from the peripheral footwall of the Hellyer deposit, but the lateral extent of such enrichment has not been determined.

(3) The down-going-limb of large convection cells, located on fossil Cambrian structures, might be recognisable as concentrations of disseminated pyrite with a seawater sulfate isotopic value. This speculation remains to be verified.

The plan of action leading from the review was to concentrate initially on verifying and defining the signature of shallow convection (point 2), by studying the periphery of another Cambrian massive sulfide, namely, the Rosebery north end footwall sulfur isotope variation.

## Previous sulfur isotope work at Rosebery

### General

It is important to examine the isotopic variation at Rosebery, as context for the values that have been obtained in this study. Previous work has established a detailed picture of sulfur isotope variation in (1) the main mineralised lenses; (2) the Devonian granite-overprint on these lenses; and (3) sulfides and sulfates of the overlying barite zone. Limited data has also been obtained from footwall sulfide veins/disseminations immediately below high grade mineralisation, and from disseminated sulfides in the hangingwall black slates. These geological units are summarised in Fig. 1.

### Base-metal sulfides and barite

The main sulfide lenses at Rosebery vary from $\delta^{34}S$ = ~7–18‰ (Solomon et al. 1969, Green 1983, Solomon et al. 1988), generally heavier than deposits in the northern Mount Read Volcanic Belt, which average ~7‰. Massive pyrite-chalcopyrite ores at Rosebery are distinctly lighter than the base-metal ores, with a mode at 9‰ (Fig. 2). This is also the case at Hercules to the south (Khin Zaw 1991). In addition, Green (1983) showed that there are distinct and systematic isotopic variations in the base metal ores, with the overall $\delta^{34}S$ value increasing (1) in the higher lenses; (2) in the upper portions of single lenses, and; (3) as a general trend southwards. Green's conclusions are based on an unfolded model of the Rosebery orebody.

Sulfide that is associated with the barite-rich ores at Rosebery have the heaviest sulfur (13–20‰), but are considered by Solomon et al. (1988) to be in equilibrium with barite (deposited at 300°C) ranging from $\delta^{34}S$ = 33–41‰, slightly above the late Cambrian seawater sulfate value (30‰).

Solomon et al. (1988) emphasise that Rosebery "is the only example in the Mount Read Volcanic Belt displaying stratigraphic zoning of $\delta^{34}S$ values (increasing with time)", which they interpret as the

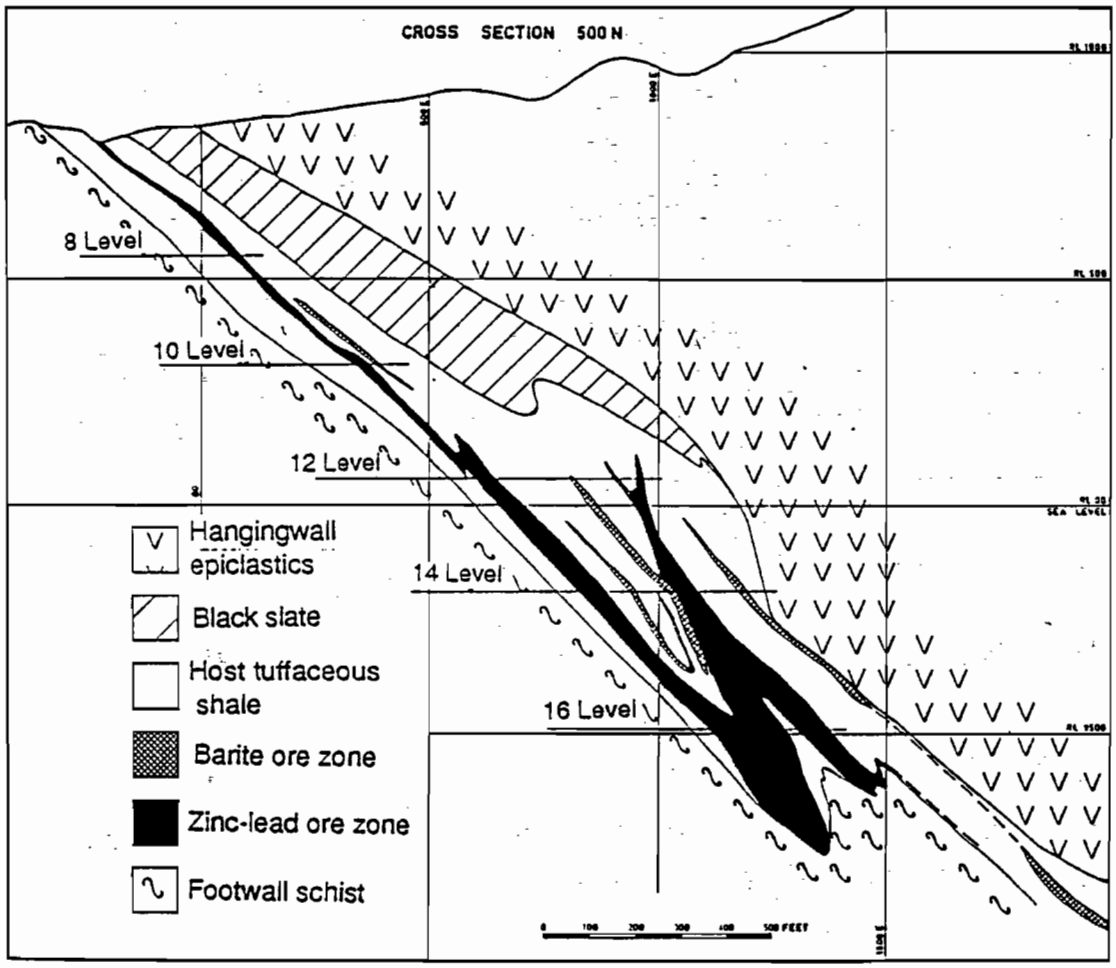


*Fig. 1. Folded geometry of the Rosebery ore lenses, after Khin Zaw (1991).*

result of an increase in the reduced seawater sulfate component, principally caused by exhaustion of available leachable rock sulfur in the deep footwall as hydrothermal circulation continued, and particularly as it began to wane. They argue that this is likely to be a widespread phenomenon in deposits with a felsic volcanic footwall, because felsic volcanics contain approximately twenty times less sulfur than basaltic rocks. This argument also explains why the Que-Hellyer sequence mineral deposits are isotopically lighter than the Rosebery area deposits. The Que-Hellyer sequence is dominated by basaltic volcanics, and hence fluids leaching it would have aquired more rock sulfur (at the same W/R) than fluid-leaching of felsic volcanics in the Rosebery area.

### Footwall alteration

Green (1983) and Solomon et al. (1969) analysed 8 pyrite-bearing veins from footwall alteration in the southern zone at Rosebery. The values varied from $\delta^{34}S$ = 10.6–14.9‰, average 12.5‰ (Fig. 3). These values were very similar to the those of directly overlying massive sulphides at this locality (Green 1983). Solomon et al. (1988), in considering these data, concluded that they indicated that shallow seawater convection within the Rosebery footwall was not likely, because there was no isotopic support for a change in oxidation state.

### Carbonaceous slate-hosted pyrite: hangingwall variation

Only three samples of hangingwall carbonaceous slate have been sampled at Rosebery previously (Solomon et al. 1969). At these sites the material analysed is referred to as "pyrite-quartz lenses parallel to cleavage", and hence is likely to represent at least locally remobilised sulfide. Repeat analysis of two samples suggested that intra-sample variation is <2‰. The isotopic range is very great, from 2.3–25.3‰. Two samples from Hercules (described as "pyrite nodules") lie within this variation, bringing the total number of analyses of this lithology to seven (Fig. 3).

### Devonian sulfur

It has been demonstrated by several workers that no isotopic change occurred as a result of the Devonian replacement of base metal sulfides by pyrrhotite during granite intrusion in the southern lodes at Rosebery (Green 1983, Solomon et al. 1988, Khin Zaw 1991). Khin Zaw found that pre-existing Cambrian variation was only homogenised at a hand-specimen scale by this process, not changed. This work suggests either that the value of Devonian sulfur was identical to the Rosebery Cambrian value, or that the general sulfur content of Devonian fluid was low, with the result that its signature was overwhelmed by Cambrian sulfur in the ore environment.

## Scope of work, and methods used

Sixty four sulfur isotopic analyses were obtained from three drillholes within and to the north of B-lens at Rosebery (Fig. 4). Laser-ablation microprobe extraction was employed after the method of Huston et al. (in press), generating sample pit diameters of ~200μ. It is this ability to sample very small grains that has been the stimulus for this research direction. However, the very small size of most grains necessitated the common practice of amalgamating the sulfur from 2–8 grains to obtain enough sulfur to measure in the mass spectrometer. Only pyrite grains were analysed in this study.

The drillholes are spaced at intervals of 0 m (hole 60R), 968 m (hole 71R), and 1781 m (107R) away from B-lens (see details in Davidson & Kitto 1994). Each intersected the hangingwall, host-sequence and the footwall lithologies, and hence represent comparable stratigraphic sections. Isotopic sampling focussed on the footwall, but also included the host and hangingwall sequences where material was available. The sample spacing was arbitrarily fixed at ~10m, but this varied widely

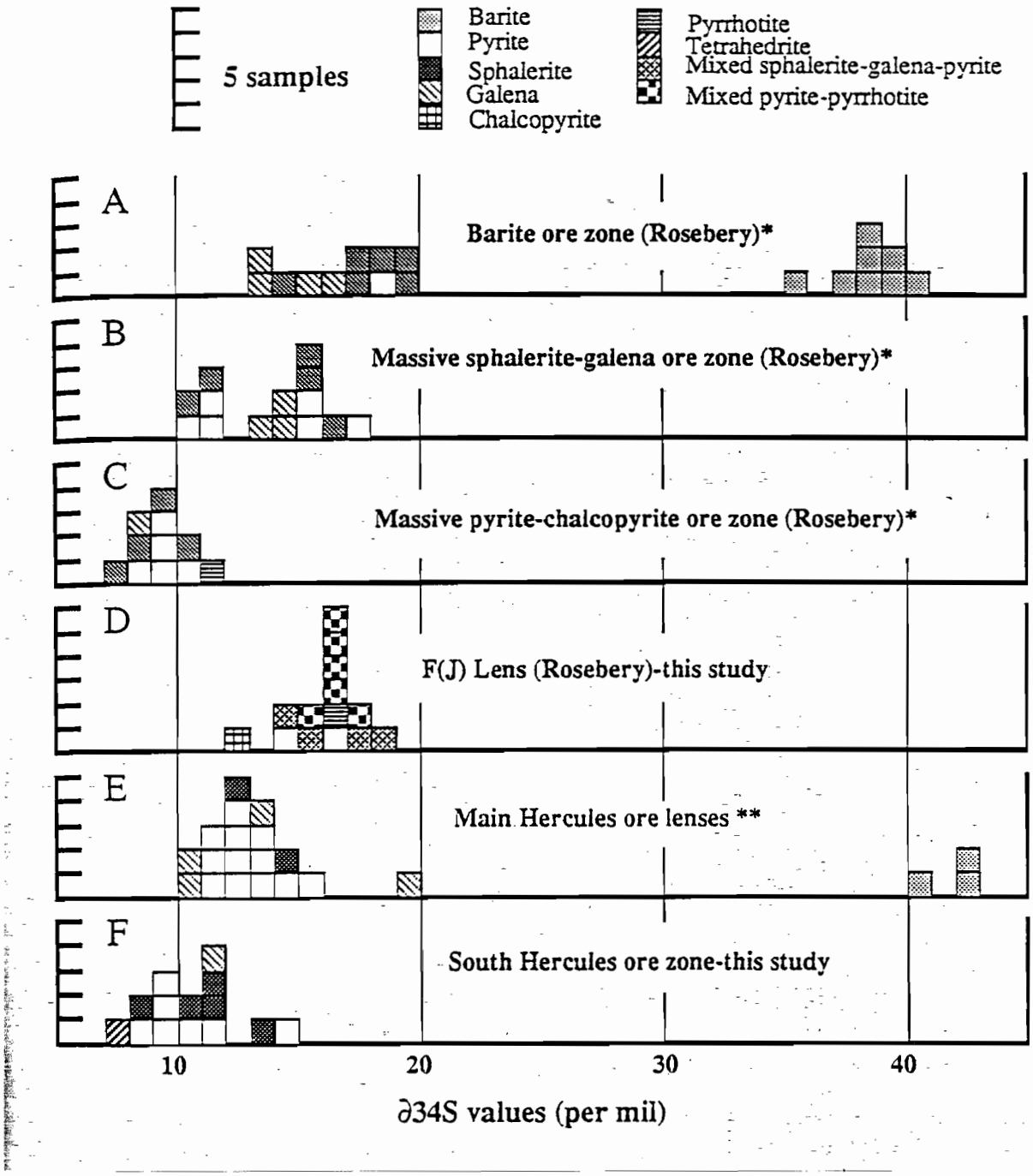


*Fig. 2. Histograms of base-metal and barite lens isotopic variation at Rosebery, after Khin Zaw (1991). [* data after Green (1983); **data after Solomon et al. (1969) and Solomon et al. (1988)].*

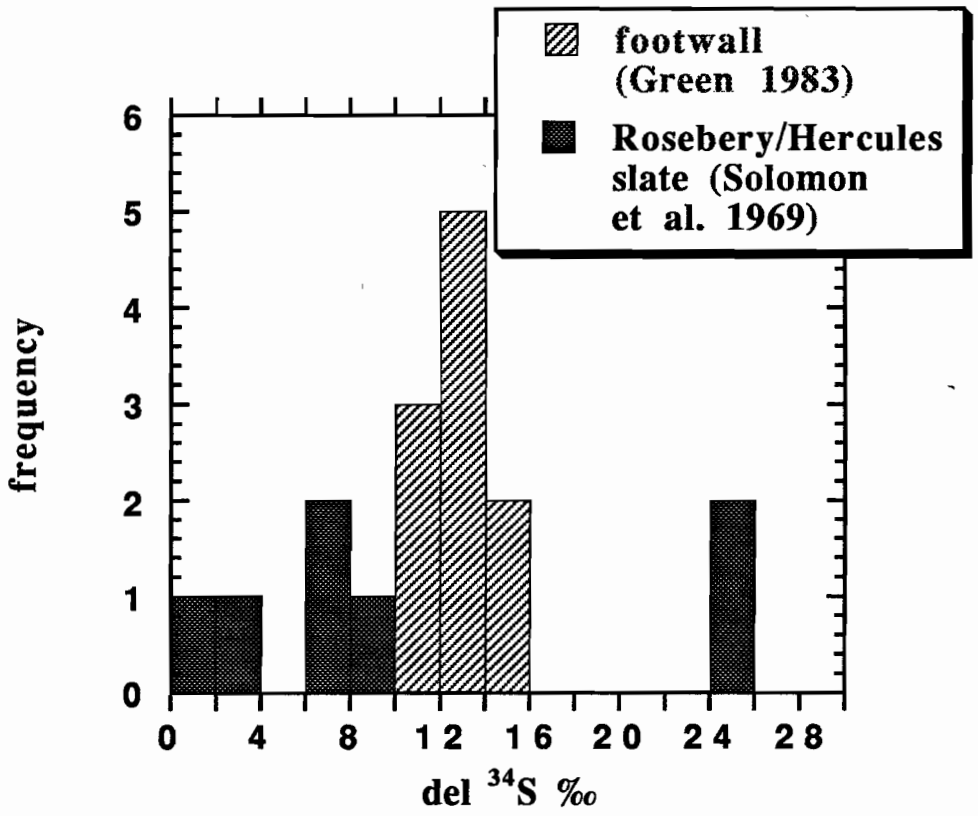


*Fig. 3. A compilation of sulfur isotope values from pyrite in Rosebery footwall alteration and carbonaceous slates.*

depending on the availability of pyrite. Experience has shown that a sample is not worth obtaining for laser ablation if sulfides are not visible with the naked eye.

A study of the pyrite morphologies has also been undertaken, because it is apparent that several pyrite forms are present in the sequence, and that these forms have characteristic isotopic signatures.

## Pyrite morphologies in the alteration zone north of B-lens

### Cambrian footwall pyrite

This is the dominant pyrite type. It forms disseminated sub- to euhedral grains with an average grain-size around 200μ, varying from ~10μ up to ~2mm. Sericite, quartz, sphalerite and galena are commonly also present. Some connected strings of this pyrite are interpreted to be deformed veins of approximately the same pyrite generation. Strong matrix pressure shadows are very common, oriented parallel to the cleavage, extending up to four grain lengths away from the pyrite crystal (Fig. 5). In the alteration beneath hole 60R, these pressure shadows may also preferentially contain pyrrhotite and sphalerite (Fig. 4) Pyrite in hole 60R commonly also contained small rounded inclusions of sphalerite and galena, which are likely to have been sampled by the laser; the inclusions are very small compared to their host grains, and are not likely to have significantly influenced the isotopic result.

In general the grain shapes and associated matrix effects are interpreted to be the result of metamorphism and ductile deformation of pyrite that had developed during Cambrian alteration.

### Devonian? footwall pyrite

A small number of samples in all three holes contained pyrite which has experienced minimal deformation. The individual grains are anhedral, with very irregular margins (verging on network morphologies), and no pressure shadowing around the grains (Fig. 5). Some of these grains are associated with carbonate, pyrrhotite and/or tourmaline, although they were not originally sampled macroscopically for this association. Most grains are between 200μ and 2mm across. In several instances ultrafine pyrite euhedra were surrounded by ragged pyrrhotite.

These features suggest this pyrite developed after the main cleavage formation, and hence must have a Devonian or post-Devonian timing. The ragged morphology may suggest the replacement of pyrrhotite by pyrite.

### *Carbonaceous slate-hosted pyrite*

Pyrite is abundant in the hangingwall black slates, where it has two dominant styles: (1) disseminated, and; (2) vein-hosted (Fig. 5). Disseminated pyrite forms sub- to euhedral crystals varying in diameter from ~50μ to 2mm, with minor associated pressure shadows, and no mineral inclusions. Vein-hosted pyrite is also sub- to euhedral, but occurs in mainly cleavage-parallel, 1–2 mm wide, quartz-carbonate veins. In places the pyrite crystals are coarser than the veins, raising the possibility that the veins have opportunistically linked between pre-existing pyrite crystals. Other crystals are entirely enclosed by veins, and appear to have grown within the vein paragenesis.

These observations suggest that if biogenic pyrite was once present in the carbonaceous slates, as would be expected for carbonaceous sediment, it has completely recrystallised to a euhedral form. The widespread association between pyrite and veining further suggests that some pyrite has also been at least locally remobilised during Cambrian/Devonian deformation.



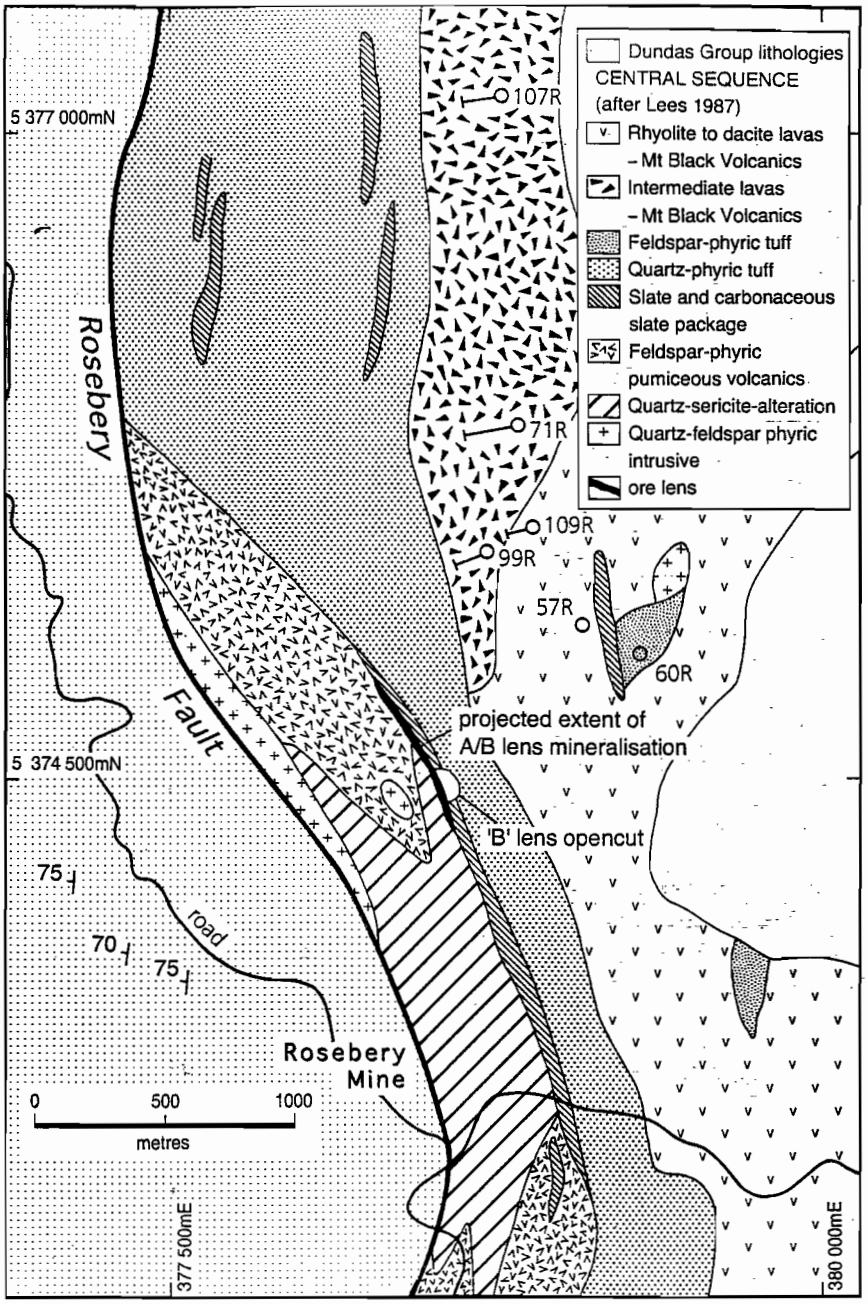


*Fig. 4. Geology of the B-lens area at Rosebery, western Tasmania, after Lees (1987).*

**OPPOSITE**

*Fig. 5. Pyrite morphologies, taken in reflected light. A. 60R/3325' (average $\delta^{34}S$ = 9.6‰) Cambrian pyrite related to alteration. Note that pyrrhotite and sphalerite have concentrated in the pyrite pressure shadow. B. 107R/722.3m (average $\delta^{34}S$ = 15.4‰). Cambrian pyrite related to alteration, with asymmetric pressure shadows. C. 71R/2133' (average $\delta^{34}S$ = 3.4‰). Very small pyrite euhedra in a pyrrhotite matrix, which is generally anhedral, and does not exhibit pressure shadowing in cleaved rocks. This assemblage is likely to have grown during Devonian granite intrusion. D. 107R/652.0m (average $\delta^{34}S$ = 3.8‰). Anhedral Devonian? pyrite, similar to 71R/2133'. The colour zonation is a relict from an adjacent laser ablation pit. E. 60R/2827'($\delta^{34}S$ = 6.7‰)[1] . Euhedral pyrite in hangingwall carbonaceous slates. F. 60R/2827'($\delta^{34}S$ = 4.6‰). Euhedral pyrite within a quartz-carbonate-pyrrhotite vein in hangingwall carbonaceous black slates.*

[1] *Labelled erroneously in the figure.*

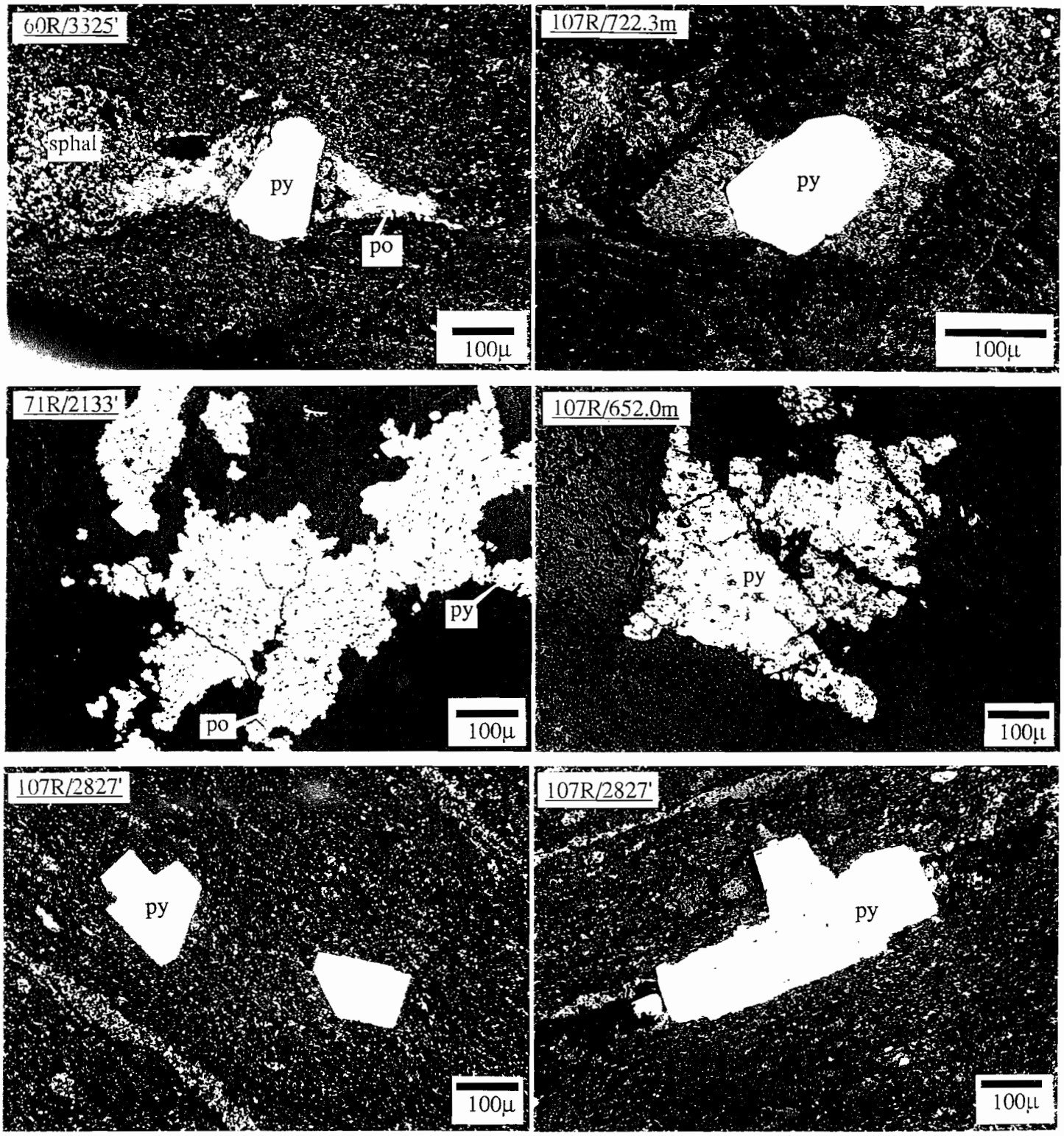
60R/3325'
sphal
py
po
100µ
107R/722.3m
py
100µ
71R/2133'
py
po
100µ
107R/652.0m
py
100µ
107R/2827'
py
100µ
107R/2827'
py
100µ

## Sulfur isotope results to date

### Reproducibility and analytical error

One problem that faces the micro-analytical approach to sulfur isotope geochemistry is demonstrating that a representative sample has been obtained. At Rosebery this was dealt with by always analysing two grains from each sample, and if the difference between the grains was great, further analyses of adjacent grains were obtained. Analyses of large grains within 1 cm of one another mainly varied by 1–2‰ (Table 1). Generally this means that in any future work at Rosebery, only one analysis is necessary (particularly if it is a composite of several small grains), but more should be made if the value obtained is significantly different to adjacent samples.

The machine and laser error for these samples, analysed using a Nd-YAG laser connected to a VG series II mass spectrometer, has been determined by numerous replicates of mineral and gas standards as 0.3–0.5‰ (Huston et al. in press).

### Footwall variation

Histograms of $\delta^{34}S$ values from the footwall sequence are presented in Fig.6, with downhole plots in Fig. 7. Only the results from Cambrian pyrite grains have been plotted on these diagrams. There is no systematic downhole variation in $\delta^{34}S$ in any of the holes (Fig. 7).

The results (Fig. 6) show that footwall pyrite immediately below B-lens (range: $\delta^{34}S$ = 7.3–17.3‰; mean $\delta^{34}S$ = 11.5‰, n = 19) is isotopically similar to sulfur from B-lens itself (9.6–10.9‰, n = 2). This mirrors the findings of Green (1983), for the southern Rosebery zone.

The same signature is present in hole 71R (970 m north of B-lens), although the number of samples was small, because sufficient sulfur was not always present. This data tentatively suggests that the ore sulfur isotope signature extends ~1 km north of the known mineralisation within the footwall. We would like to do more analyses to confirm this.

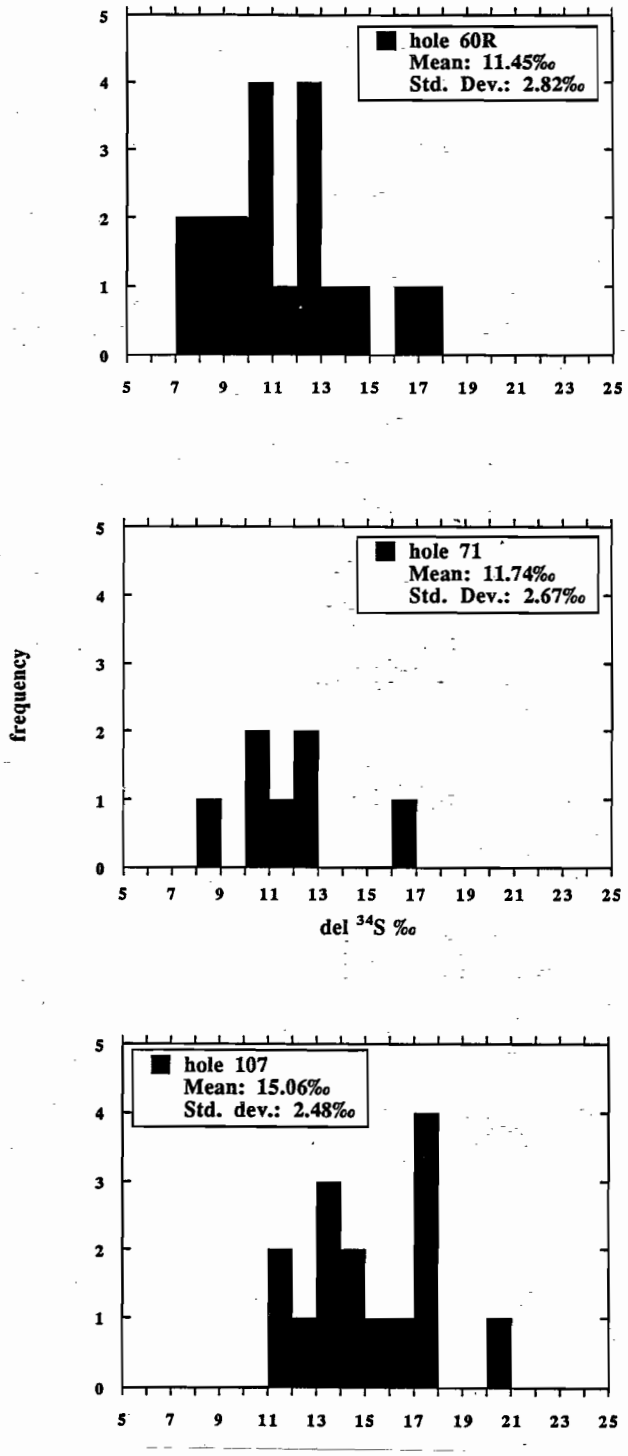


*Fig. 6. Histograms of Cambrian footwall pyrite $\delta^{34}S$ variation north of B-lens.*

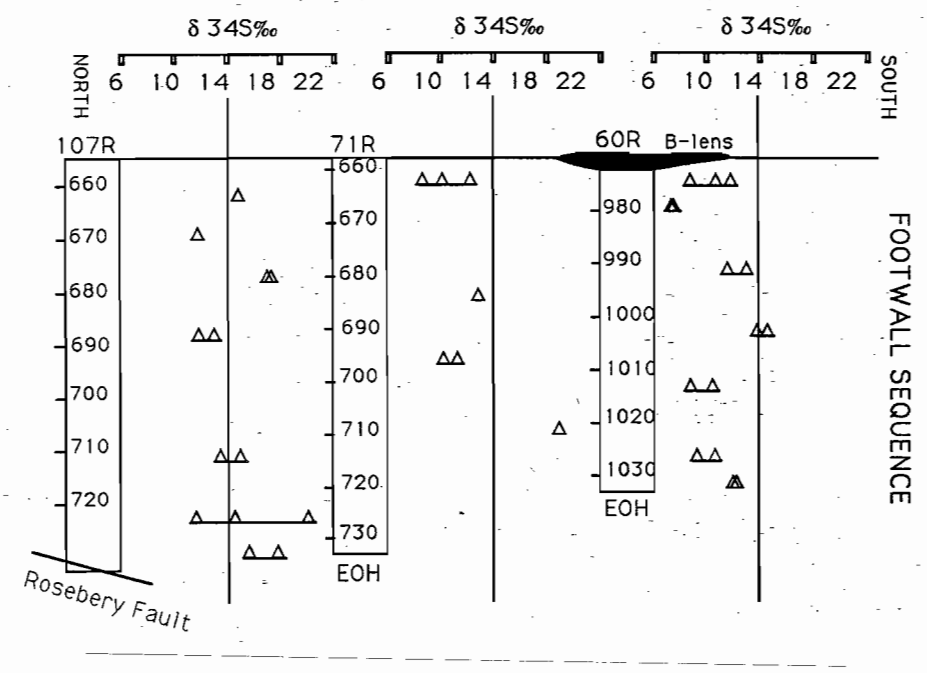


*Fig. 7. Downhole plots of $\delta^{34}S$ from Cambrian footwall pyrite in this study. Only downhole metreages have been used. The plot shows that there is no systematic variation in downhole $\delta^{34}S$ for any hole.*

The variation in hole 107R is distinctly heavier than in the other holes. The data ranges between 11.8 and 20.2‰, with a mean of 15.1‰ (n = 13).

### Black slate

Disseminated euhedra in this unit varied from 8.8–19.2‰ (n = 6), whereas vein pyrite varied from 4.6–15.9‰ (n = 10). Where it has been possible to compare the variation of vein and disseminated pyrite in the same sample (60R-2827, 60R-2890), the vein pyrite was up to 4‰ lighter (Fig. 8), suggesting some mixing with lighter sulfur during vein formation. However, given that the veins display the same total isotopic variation, they are regarded mainly as the product of local remobilisation. This was not a systematic part of our study, so that further work is warranted to confirm the result. This is not a priority objective. The result must be viewed cautiously, given that vein pyrite can vary 5‰ in a single grain (71R-1707; Table 1).

### *Devonian? pyrite*

Post-cleavage pyrite varied isotopically from 1.1‰ to 3.8‰ (n=4). These values are well outside the range of Cambrian variation at Rosebery. Given the association of the pyrite with carbonate and pyrrhotite, these values may represent the value of Devonian granite-related sulfur.

## Discussion

The most important finding of the study to date is the distinct increase of footwall $\delta^{34}S$ in hole 107R, 1.8 km north of B-lens.

This increase occurs across the entire sampled stratigraphic sequence. It is comparable in magnitude to the isotopic value of sulfides in the barite zones at Rosebery (Green 1983), and must signal a lateral increase in the amount of reduced seawater sulfate that was deposited from a circulating Cambrian hydrothermal fluid. This confirms the idea that shallow seawater convection can be traced using sulfur isotopes, which was the aim of the isotopic work at Rosebery. However, the extent of

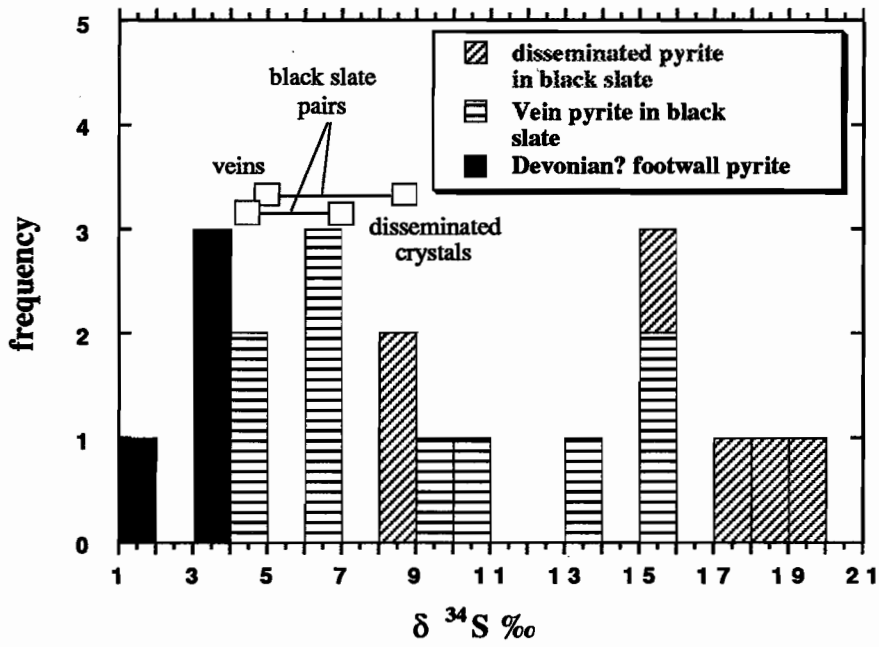


*Fig. 8 Sulfur isotopic variation of pyrite in hangingwall black slate, and probable Devonian pyrite with anhedral morphologies in the Rosebery footwall.*

isotopic increase is less than at Hellyer, where Gemmell & Large (1993) found peripheral stringer zone sulphide-bearing veins ranging from 11.9–40.7‰ (mean of 25.0‰; Stage 2A), and Jack (1989) found pyrite in the footwall andesites, just outside the stringer envelope zone, to be distinctly heavy (23.0–27.0‰) compared to the Hellyer ore values (5.3–9.4‰).

One means of explaining the difference in the scale and extent of the isotopic change between the two deposits is the different nature of the footwall rocks. At Hellyer it is now well documented that the footwall rocks consisted of submarine coherent basaltic lavas. The low porosity of this unit presumably was the major reason that the Hellyer ores formed a discrete mound overlying a distinctly focussed alteration pipe. In contrast, recent workers (e.g., Allen & Cas 1990, McPhie & Allen 1992), have shown that the Rosebery footwall consisted of thick tube-pumice breccias. As pointed out by Huston (1989), the porous character of these breccias lead to alteration being dispersed rather than focussed, which may account for the sheet-like character of the ore. In this porous subsurface, it is not surprising that the gradation from the rock-sulfur-dominated hydrothermal fluid zone, to peripheral zones of shallow seawater convection, should have occurred over a comparitively greater distance than at Hellyer. The greater porosity would also have permitted greater mixing between the main hydrothermal upflow and peripheral convection cells, which would cause a more gradual change in the sulfur isotope values of hydrothermal pyrite.

This work is confirming the notion that seawater sulfate reduction occurs marginal to the upwelling limb of deep convection cells. For this to be accomplished, the sulfate must be heated to ≥200°C (Ohmoto & Lasaga 1982), where it is reduced by reaction with ferrous iron in the host-rock. Porous lithologies such as the Rosebery footwall would provide naturally high W/R conditions which promoted fluid access to iron phases, and hence assisted reduction. However, only partial sulfate reduction occurred, because the rate of reaction at



these temperatures is comparitively slow. The data at Rosebery suggest that the seawater must have been rapidly reduced, to prevent the deposition of isotopically light sulfur, which would occur if a given batch of fluid remained near the $SO_4/H_2S$ species boundary. Very light sulfur values would certainly be expected in the cooler and near-surface parts of the peripheral convection cell, as suggested by Solomon et al. (1988) to account for values lower than 5‰ at Cambrian systems such as Chester, Howards Anomaly, and Basin Lake.

## Implications for Cambrian structures

This work suggests that Cambrian structures which experienced medium temperature (~200°C) seawater circulation can be identified on the basis of sulfur isotopes in pyrites. The geometry and size of the isotopic anomalies in such zones must still be established.

## Work in progress

1. A second phase of the Rosebery work is to refine the sulfur isotope pattern by examining infill-holes, and also to further define the Devonian fluid signature by analysing sulfur from the Rosebery fault. The samples for this work are currently being prepared.
2. Work will be extended to other Cambrian structures, which have been identified from other criteria by members of the research group. An additional approach will be an experimental evaluation of $Fe^{2+}/Fe^{3+}$ ratios in the same rocks, as a sensitive indicator of the fossil reduction of seawater sulfate.

## Suggestions for sulfur isotope work in the geochemical haloes project

1. Systematic analysis of vein and disseminated pyrite in the black slate.

   It is possible that Cambrian VHMS fluids continued to permeate into the carbonaceous shale cap at Rosebery after the cessation of base metal deposition, which may have systematically altered the isotopic composition of intra-shale biogenic pyrite. This possibility requires careful along- and cross-strike isotopic analysis which is beyond the scope of the Cambrian structures project. This work would have implications for the exploration of other shale-hosted basins in the Mount Read Volcanic Belt, and elsewhere.

2. Detailed delineation of the footwall sulfur isotope distribution in areas of recognised Devonian fluid overprint at Rosebery.

3. Extending the microanalytical sulfur isotope approach to Hellyer and Que River (and other massive sulphide deposits??), particularly to determine the ***extent*** of peripheral sulfur isotope enrichment, which is presently unknown.

4. Determination of the Co/Ni ratio for pyrites in this study, to compare to the work of Green (1983), who found that Co/Ni in pyrite was a sensitive indicator of fluid change in the Rosebery footwall.

5. Examine materials with a view to extending the footwall sulfur isotope coverage at Rosebery.

## Conclusions

$\delta^{34}S$ values of footwall pyrite 1.8 km north of B-lens at Rosebery confirms that the proportion of seawater sulfate-derived sulfur increases away from the main alteration zone, which is attributed to shallow Cambrian seawater convection around the main upflow limb of a deep convective cell. All previous work on footwall pyrite at Rosebery had indicated that it was isotopically similar to the mineralised lenses. This confirms observations made previously at Hellyer. The increase in $\delta^{34}S$ values occurs further from ore, and is not as pronounced, as at Hellyer. These differences are attributed to the original highly porous character of

the Rosebery footwall, and leads to the general conclusion that fluid flow in the felsic breccias (which are widespread in the Mount Read Volcanic Belt) was more diffuse than in coherent lava sequences such as the Que-Hellyer belt.

Sulfur isotope values can be used to identify Cambrian structures which have experienced medium temperature (~200°C) seawater circulation. At these temperatures seawater sulfate will be at least partially reduced, and new pyrite will be significantly heavier than ambient igneous pyrite in volcanic rocks (probably $\delta^{34}S = 4 \pm 4‰$; Davidson & Kitto 1994).

## References


Allen R.L. & Cas R.A.F. (1990) The Rosebery controversy: distinguishing prospective submarine ignimbrite-like units from true subaerial ignimbrites in the Rosebery-Hercules ZnCuPb massive sulfide district, Tasmania. Geol. Soc. Aust. Abs. 25: 31–32.

Davidson G.J. & Kitto P. (1994) Sulfur isotopes as a guide to Cambrian structures in the Mount Read Volcanics — first progress report. AMIRA Project P.291A — Structure and mineralisation of Western Tasmania, May 1994: 67–75.

Gemmell J.B. & Large R.R. (1993) Evolution of a VHMS hydrothermal sytstem, Hellyer deposit, Tasmania, Australia: sulphur isotope evidence. Resource Geology Special Issue 17: 108–119.

Green G.R.(1983) The geological setting and formation of the Rosebery volcanic-hosted massive sulphide orebody, Tasmania. Ph.D thesis, University of Tasmania (unpublished). 288 p.

Huston D.L. (1989) Aspects of the geology of massive sulphide deposits from the Balcooma district, northern Queensland and Rosebery, Tasmania: Implications for ore genesis. Ph.D thesis (unpublished), University of Tasmania. 380 p.

Huston, D.L., Power M., Gemmell J.B. & Large R.R. (in press) Design, calibration and geological application of the first operational Australian laser ablation sulphur isotope microprobe. Aust. J. Earth Sci.

Jack D.J. (1989) Hellyer host rock alteration. M.Sc. thesis (unpublished), University of Tasmania. 182 p.

Khin Zaw (1991) The effect of Devonian metamorphism and metasomatism on the mineralogy and geochemsitry of the Cambrian VMS deposits in the Rosebery-Hercules district, western Tasmania. Ph.D thesis, University of Tasmania (unpublished).

Lees T. (1987) Geology and mineralisation of the Rosebery-Hercules area, Tasmania. M.Sc thesis, University of Tasmania (unpublished). 184 p.

McPhie J. and Allen R.L. (1992) Facies architecture of mineralized submarine volcanic sequences: Cambrian Mount Read Volcanics, Western Tasmania. Econ. Geol. 87: 587–596.

Ohmoto H. & Lasaga A.C. (1982) Kinetics of reactions between aqueous sulfates and sulfides in hydrothermal systems. Geochim. Cosmochim. Acta 46: 1727–1745.

Solomon M., Rafter T.A. & Jensen M.L. (1969) Isotope studies on the Rosebery, Mount Farrell and Mount Lyell ores, Tasmania. Minera. Deposita 4: 172–199.

Solomon M., Eastoe C.J., Walshe J.L. & Green G.R. (1988) Mineral deposits and sulfur isotope abundances in the Mount Read Volcanics between Que River and Mt Darwin, Tasmania. Econ. Geol. 83: 1307–1328.




*Table 1 Sulfur isotope values obtained in this study only; Rosebery footwall, host-rock sequence, and hangingwall rocks.*

| DDH/metreage | anal. no. | del 34S ‰ | del 34S ‰ | Stratigraphic position | Comment |
|---|---|---|---|---|---|
| | | | Average/sample | | Grain-size is noted in μ |
| | | | | | |
| **DDH 107R** | | | | | |
| 107R-546.6m | 1048 | 6.26 | 7.60 | Black Slate | Vein py edge |
| | 1049 | 8.94 | | | Vein py centre |
| 107R-558.5m | | | | Black Slate | |
| 107R-601.1m | | | | HW epiclastics | |
| 107R-621.0m | | | | HW epiclastics | |
| 107R-639.7m | | | | HW epiclastics | |
| 107R-651.4m | 1052 | | | Host sequence | Too small |
| | 1053 | 16.01 | 16.64 | | 1mm py vein, Cambrian |
| | 1054 | 17.27 | | | Same vein; 1cm to 1053 |
| 107R-652.5m | 1069 | 3.84 | 3.84 | Host sequence | Anhedral clot 2mmx3mm: Dev.? |
| 107R-661.1m | 1070 | 15.07 | 15.07 | FW volcanics (Pumiceous Breccia) | Recryst. Cambrian py; 200μ av. |
| 107R-669.9m | 1082 | 12.63 | 12.63 | FW volcanics (Pumiceous Breccia) | Recryst. Cambrian py; 70μ av. |
| | 1083 | | | | Too small |
| 107R-677.3m | 1064 | 17.01 | 17.01 | FW volcanics | Recryst'd py; 400μ av. |
| | 1065 | 17.00 | | | Recryst'd py; 400μ av. |
| 107R-688.3m | 1073 | 11.77 | 12.42 | FW volcanics (Pumiceous Breccia) | Recryst'd py; 400μ av. |
| | 1074 | 13.07 | | | Recryst'd py; 100μ av. |
| 107R-711.1m | 1071 | 14.99 | 14.15 | FW volcanics (Pumiceous Breccia) | Recryst'd py; 400μ av. |
| | 1072 | 13.30 | | | Recryst'd py; 400μ av. |
| 107R-722.3m | 1066 | 20.18 | 15.41 | FW volcanics (Pumiceous Breccia) | Recryst'd py; 700μ av. |
| | 1067 | 11.76 | | | Recryst'd py; 700μ av. |
| | 1068 | 14.29 | | | Recryst'd py; 100μ av. |
| 107R-728.0m | 1051 | 13.55 | 15.75 | FW volcanics (Pumiceous Breccia) | Recryst'd py; 500μ av. |
| | 1050 | 17.95 | | | Recryst'd py; 300μ av. |
| **DDH 71R** | | | | | |
| 71R-1648.0' | 1003 | 17.10 | 16.21 | Black Slate | Primary 4mm grain |
| | 1004 | 15.32 | | | Primary 0.5mm grain |
| 71R-1707.0' | 995 | 15.94 | 14.15 | Black Slate | Gape-fill: single crystal |
| | 996 | 10.88 | | | 500 μ from 995; same crystal |
| | 997 | 15.48 | | | thin short vein; 0.5cm from 995 |
| | 998 | 13.06 | | | thin short vein; 1 cm from 995 |

| DDH/metreage | anal. no. | del 34S ‰ | del 34S ‰ | Stratigraphic position | Comment |
|---|---|---|---|---|---|
| | | | Average/sample | | Grain-size is noted in μ |
| | 999 | 15.39 | | | same vein as 998; 300μ away |
| 71R-2096.5' | | | | HW epiclastics | |
| 71R-2107.0' | 1005 | 1.13 | 1.13 | HW epiclastics | Anhedral 2mm grain...Devonian? |
| | 1006 | | | | Sample too small |
| 71R-2133.0' | 1042 | 3.56 | 3.35 | Host sequence | Filagree pyrite....Devonian? |
| | 1043 | 2.96 | | | Filagree pyrite....Devonian? |
| 71R-2174.0' | 1075 | 8.65 | 10.74 | Host Sequence | recrystallised py;250μ av. |
| | 1076 | | | | Sample too small |
| | 1079 | | | | Sample too small |
| | 1080 | 12.20 | | | recrystallised py;250μ av. |
| | 1081 | 10.43 | | | recrystallised py;250μ av. |
| 71R-2210.0' | 1040-1041 | | | FW Volcanics | Sample too small |
| 71R-2245.0' | 1056 | 12.72 | | FW Volcanics | recrystallised py xtal; 50μ av. |
| | | | | | |
| 71R-2286.0' | 1044 | 10.17 | 10.60 | FW Volcanics | recrystallised py xtal; 2–300μ |
| | 1045 | 11.03 | | | recrystallised py xtal; 2–300μ |
| 71R-2325.0' | 1057 | 16.97 | 16.97 | FW Volcanics | recrystallised py xtal; 50μ av. |
| | | | | | |
| 71R-2351.0' | 1000-1002 | | | FW Volcanics | Sample too small |
| **DDH 60R** | | | | | |
| 60R-2827.0' | 1035 | 4.60 | 5.64 | Black Slate | Vein in black shale: 3 large gns. |
| | 1036 | 6.68 | | | 8 disseminated grns, 50–100μ |
| 60R-2850.0' | 1032 | | | Black Slate | Too small |
| | 1033 | 18.37 | 18.80 | | Recryst'd & dissem'd;large grains |
| | 1034 | 19.23 | | | Recryst'd & dissem'd;large grains |
| 60R-2890.0' | 1013, 15, 17 | | | Black Slate | Too small |
| | 1014 | 5.98 | 5.05 | | Vein pyrite in black shale |
| | 1016 | 8.75 | 8.75 | | Recrystallised euhedra; 100μ av. |
| | 1018 | 8.80 | | | Recrystallised euhedra; 500μ av. |
| | 1019 | 4.12 | | | Vein py, 2 grains |
| 60R-3001.0' | 1024 | -4.37 | -4.01 | Porphyry???? | Recryst'd;100μ av. |
| | 1025-1027 | | | | Too small |
| | 1028 | -3.66 | | | Big euhedra in deformed vein |

| DDH/metreage | anal. no. | del 34S ‰ | del 34S ‰ | Stratigraphic position | Comment |
|---|---|---|---|---|---|
| | | | Average/sample | | Grain-size is noted in μ |
| 60R-3095.0' | 1031 | 9.64 | 9.64 | Ore Zone | Massive pyrite; analysed one gn |
| 60R-3106.0' | 1039 | 10.90 | 10.90 | Ore Zone | Abundant pyrite, recrystallised |
| | | | | | |
| 60R-3154.5' | 1058 | 16.89 | 17.25 | FW Volcanics | Recrystallised;150μ |
| | 1059 | 17.46 | | | Recrystallised;150μ |
| 60R-3197.0' | 1010 | 8.98 | 10.56 | FW Volcanics | Recrystallised, single gn; 300μ |
| | 1009 | | | | Too small |
| | 1011 | 12.01 | | | Recrystallised, single gn; 300μ |
| | 1012 | 10.70 | | | Recrystallised, single gn; 200μ |
| 60R-3213.0' | 1029 | 7.19 | 7.25 | FW Volcanics | Recrystallised, single gn; 500μ |
| | 1030 | 7.29 | | | Recryst'd; 800μ; 1cm from 1029 |
| 60R-3253.0' | 1022 | 12.94 | 12.29 | FW Volcanics | Recrystallised, single gn; 1000μ |
| | 1023 | 11.65 | | | Recrystallised, two gn;400μ |
| 60R-3290.0' | 1007 | 13.79 | 14.09 | FW Volcanics | Recrystallised, single gn;200μ |
| | 1008 | 14.39 | | | Recrystallised, single gn;200μ |
| 60R-3325.0' | 1020 | 10.49 | 9.56 | FW Volcanics | Recrystallised, two gn;400μ |
| | 1021 | 8.63 | | | Recrystallised, single gn;400μ |
| 60R-3346.0' | | | | FW Volcanics | |
| 60R-3368.0' | 1037 | 9.23 | 10.06 | FW Volcanics | Recrystallised, 5 gns;150μ |
| | 1038 | 10.90 | | | Recrystallised, 3 gns;150μ |
| 60R-3385.0' | 1046 | 12.55 | 12.28 | FW Volcanics | Recrystallised;150μ |
| | 1047 | 12.01 | | | Recrystallised;200μ |

# Stratigraphy and palaeovolcanology of the Cambrian Tyndall Group, Mount Read Volcanics, western Tasmania

**Matthew J. White**

*Centre for Ore Deposit and Exploration Studies*

## Abstract

The Tyndall Group comprises dominantly felsic to intermediate redeposited volcaniclastic mass-flow deposits, accompanied by minor felsic pyroclastic flow deposits, felsic to intermediate coherent lavas and/or intrusions and non-volcanic sedimentary rocks. The Group extends from near Mount Darwin in the south, to near Mount Read. Correlates of the Tyndall Group have been identified in the upper part of the Mount Charter Group, around the Cradle Mountain Link Road, ~3 km northeast of Hellyer (Corbett 1992). This sequence correlates well with Tyndall Group sequences further south. The Tyndall Group constitutes the upper part of the Mount Read Volcanics, and in places is conformably overlain by the Late Cambrian to Early Ordovician Owen Conglomerate. The Tyndall Group has been moderately affected by low grade greenschist to prehnite-pumpellyite facies regional metamorphism and/or diagenetic alteration and compaction.

Although the internal stratigraphy of the Tyndall Group is complex, a three-fold informal subdivision is generated, consisting of the basal Comstock Tuff, the upper Comstock Tuff, and the overlying upper Tyndall Group sequences. The subdivisions are based on contrasting lithology and composition, which largely reflect different provenance characteristics. The subdivisions are regionally extensive in the central Mount Read Volcanic belt. The basal Comstock Tuff consists of dominantly syn-eruptive, andesitic to dacitic, crystalilithic volcaniclastic mass-flow units and turbidites, together with minor laminated mudstone, carbonate and volcaniclastic lithic breccia. The upper Comstock Tuff is rhyolitic to dacitic in character, and is dominated by syn-eruptive, crystal ± llithic volcaniclastic mass-flow units, with minor felsic welded ignimbrite and felsic lavas (and/or intrusives). The upper Tyndall Group consists of post-eruptive, polymict volcaniclastic conglomerate and sandstone units.

The volcaniclastic units that dominate the Tyndall Group are interpreted as resedimented subaqueous mass-flow units and turbidites, indicating transportation and deposition by low- to high-density turbidity currents and/or debris flows, in a below-storm-wave-base submarine environment. However, the local presence of an *in situ* limestone unit at Comstock containing abundant shallow marine fossils (Jago et al. 1972) and an *in situ* welded ignimbrite unit at Zig Zag Hill (Corbett et al. 1974; White et al. 1993) suggest that part of the group was deposited in shallower water, in proximity to subaerial environments.

Sources of the volcaniclastic components in the Tyndall Group are not exposed or have been eroded away. However, syn-eruptive resedimented volcaniclastic deposits and primary pyroclastic flow deposits (welded ignimbrite) in the basal and upper Comstock Tuff sequences, provide a record of the character and setting of volcanic activity in the



source. The high proportion of juvenile pyroclasts (e.g. crystals, crystal fragments, shards, pumice) within the syn-eruptive volcaniclastic facies, and occurrences of welded ignimbrite, indicate explosive magmatic and/or phreatomagmatic eruptions in the source, and suggests that the source volcanic centres were subaerial to shallow marine. Pyroclasts were probably transported to the marine basin by pyroclastic flows which transformed into water-supported mass flows on entry into water, and finally deposited below storm wave base. During transportation fine ash was driven off into secondary ash plumes generated at the shoreline, and into ash-rich suspensions associated with the ensuing subaqueous volcaniclastic mass flows (cf Cas 1983). The initial eruptions were andesitic to dacitic, leading to deposition of the plagioclase-clinopyroxene-magnetite dominated units of the basal Comstock Tuff. Rhyolitic to dacitic eruptions followed leading to quartzplagioclase rich mass-flow deposits of the upper Comstock Tuff. Ignimbrite was deposited in subaerial to shallow marine parts of the basin from the subaerial pyroclastic flows. Some of the ignimbrite deposited in shallow water environments contributed clasts (some up to several 10's m across) that were subsequently transported down slope, and together with crystal and lithic components, formed giant subaqueous mass flows (White et al. 1993).

The upper Tyndall Group volcaniclastic facies contains abundant rounded volcanic lithic (and other) clasts, indicating erosion and reworking in high energy environments (prior to redeposition by subaqueous mass flows), and that the source areas were subaerial to shallow marine. Tectonic uplift may have increased erosion rates in the source, producing the large proportion of epiclasts present in this facies. This uplift eventually exposed Precambrian basement rocks, feeding Precambrian quartzite clasts into the basin, as seen in the upper parts of the upper Tyndall Group.

The overall palaeogeographic setting of the Cambrian Tyndall Group is similar to that in the eastern to central parts of the North Island of New Zealand and the adjacent marine basins (e.g. Harve Trough). Active subaerial volcanic centres in the Taupo Volcanic Zone, produce enormous volumes of volcanic debris, and lie in proximity to the sea. Both primary pyroclastic processes (flows, fallout) and secondary processes (fluvial, etc.) have delivered volcanic debris to the sea, depositing large volumes offshore.

## References

Cas RAF (1983) Submarine 'crystal tuffs': their origin using a lower Devonian example from southeastern Australia. Geol Mag 120: 471-486.

Corbett KD (1992) Stratigraphic-volcanic setting of massive sulfide deposits in the Cambrian Mount Read Volcanics, Tasmania. Econ Geol 87: 564-586.

Corbett KD, Ried KO, Corbett EB, Green GR, Wells K and Sheppard NW (1974) The Mount Read Volcanics and Cambrian-Ordovician relationships at Queenstown, Tasmania. J Geol Soc Aust 21:173-186.

Jago JB, Reid KO, Quilty PG, Green GR and Daily B (1972) Fossiliferous Cambrian limestone from within the Mount Read Volcanics, Mount Lyell Mine area, Tasmania. J Geol Soc Aust 19: 379-382.

White MJ, McPhie J, Corbett KD and Pemberton J (1993) Welded ignimbrite emplaced below wave base: Cambrian examples in Tasmania. IAVCEI General Assembly, Canberra Abstracts: p121.

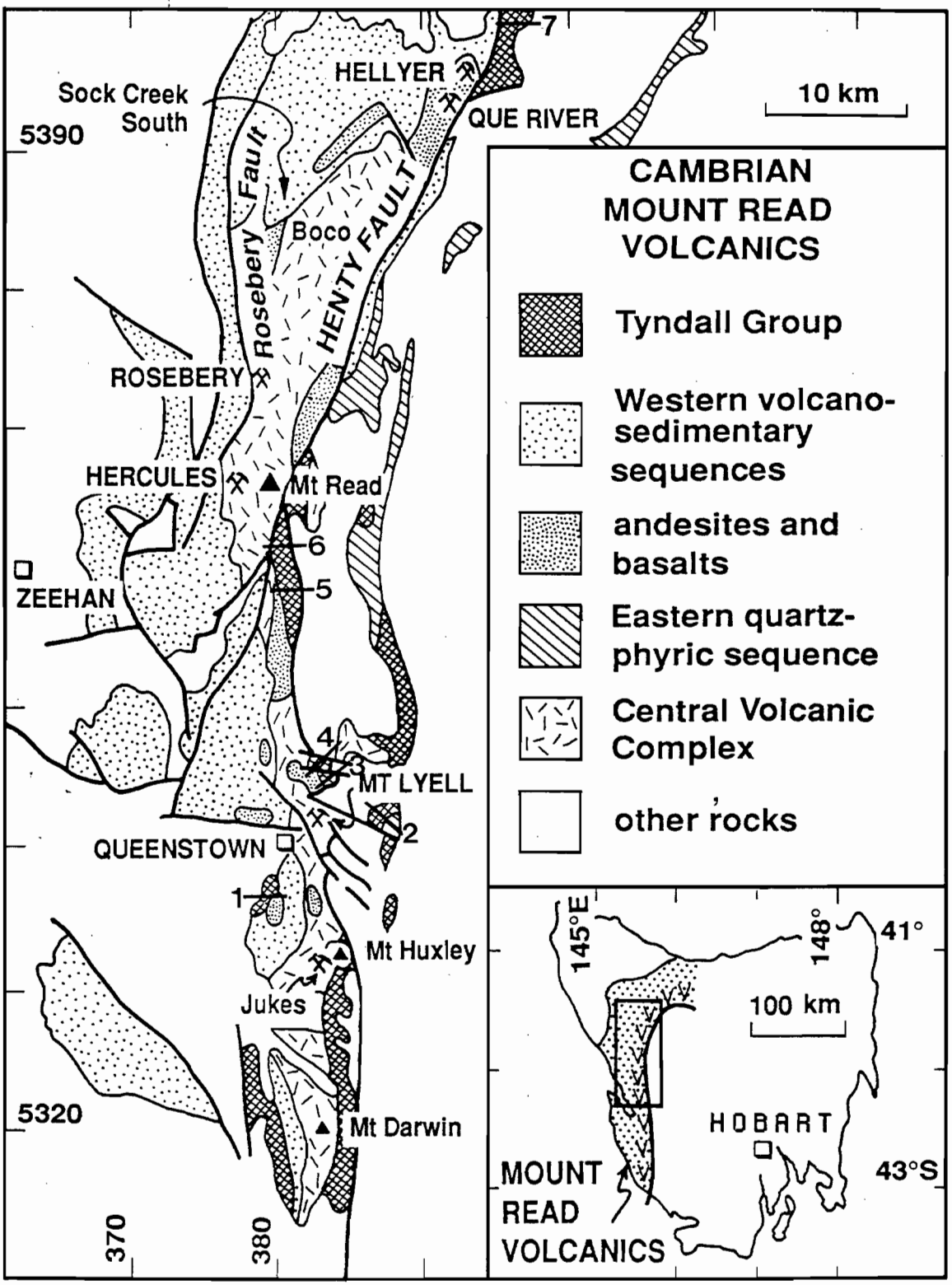


*Fig. 1 Distribution of the Tyndall Group and other principal lithostratigraphic units of the Mount Read Volcanics, and the location of seven major Tyndall Group sequences analysed. 1. Lynchford, 2 East Mount Lyell, 3 Comstock, 4 Zig Zag Hill, 5 Anthony Road, 6 Henty Canal, 7 Cradle Mountain Link Road.*

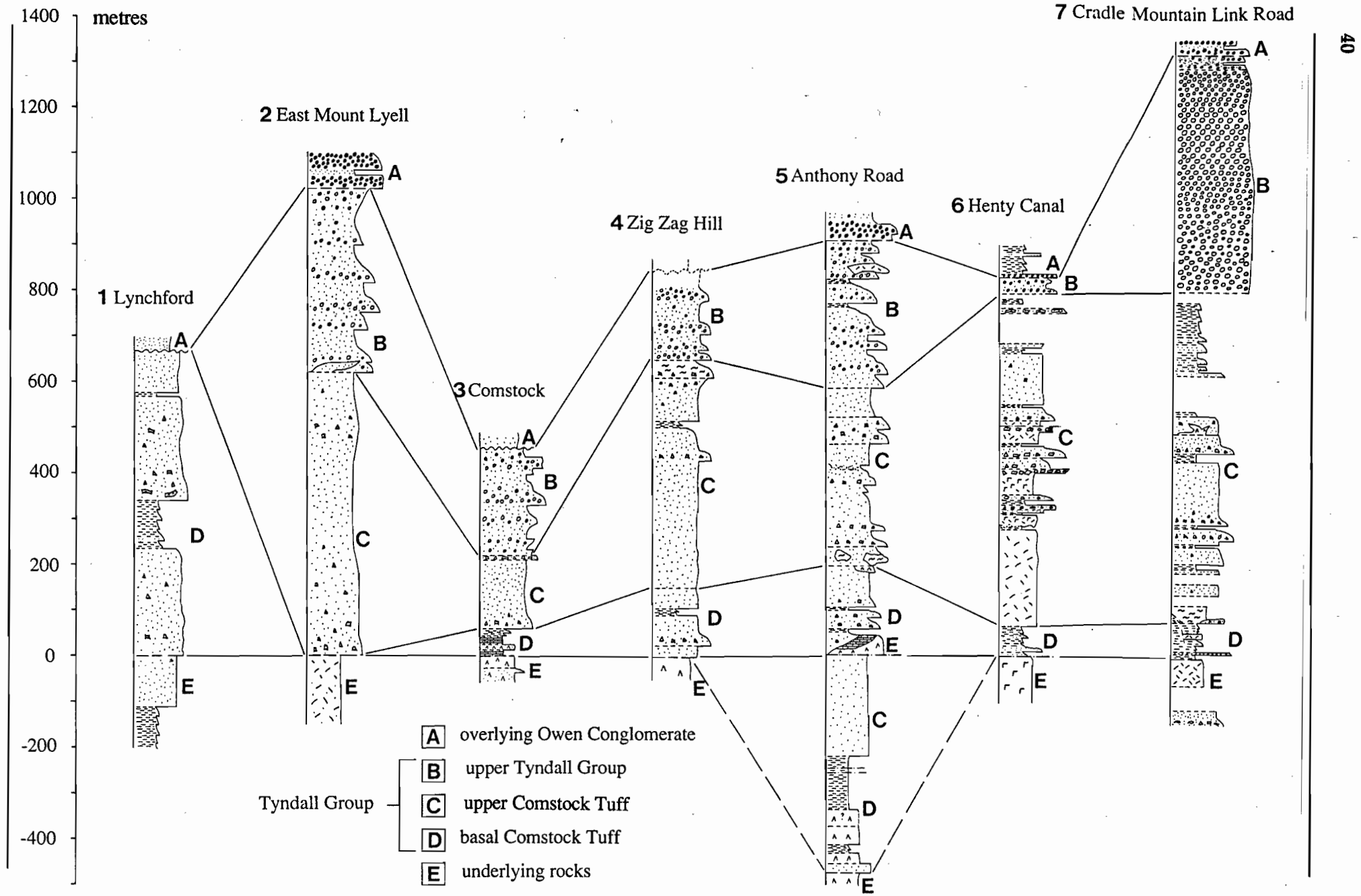


*Fig. 2. Stratigraphy and correlation — Cambrian Tyndall Group*

# Depositional Cycles of the Dundas Group

**David Selley**

*Centre for Ore Deposit and Exploration Studies*

The Dundas Group comprises the western-most portion of the Middle to Late Cambrian Mt Read volcanic belt (Fig. 1). It consists of a turbidite-dominated succession that rests unconformably upon a basement of intercalated basaltic pillow lavas and volcanic breccias. The underlying volcanic sequence occurs as part of the Serpentine Hill Complex, which is considered to be an allochthonous fragment of intra-oceanic forearc crust, tectonically emplaced onto a Late Proterozoic passive margin sequence during the Middle Cambrian (Crawford and Berry, 1992).

The succession is characterised by rapid vertical and lateral facies changes, ubiquitous soft sediment deformation, disappearance and reappearance of formations along strike and out-of-sequence stratigraphic relationships. In addition to these complexities, a further episode of disruption resulting from brittle faulting during the Devonian phase of orogenesis makes regional stratigraphic correlations extremely difficult. In order to establish a coherent depositional history therefore, a simplification of the formal stratigraphy is required. This has been achieved via a broad subdivision, where packages of strata exhibiting similar lithofacies associations, detrital composition, fossil ages and style of deformation are grouped into one of three depositional cycles (*Cycles A-C*) (Table. 1). The distribution of sediments deposited within each cycle is shown in Fig. 1. *Cycles B* and *C* are confined to the W and SW of the NNE trending Great Northern Fault. Conversely, sediments within *Cycle A* are thickest in the hangingwall of this structure, but also occur as highly tectonised lozenges and blocks within the central part of the region, where they are intercalated with *Cycle B* deposits.

***Cycle A* (mid. Middle C–Late Middle C):**
Deposition is considered to be coeval with active Mt Read volcanism as indicated by the intercalation of syn-eruptive volcaniclastic deposits (pumiceous mass-flow deposits and feldspar-phyric crystal rich sandstone) with fine and medium-grained sedimentary units. The presence of micaceous, quartz-rich sandstones and chert-dominated conglomerate implies that basement lithologies also served as a significant source. Towards the end of the cycle, introduction of minor sedimentary lithic detritus indicates a transition into the dominantly intrabasinally sourced sediments of *Cycle B*.

***Cycle B* (late Middle C–early Late C):**
A period of basin closure is indicated by the reworking of intrabasinal lithologies and localised uplift and erosion of basement. Sedimentation during this cycle was fed mainly through a system of subaqueous fans which deposited sheet-like bodies of closed framework, polymict conglomerate and interchannel fine grained turbidites. Pulses of mass-failure deposition in the form of debris flows and talus breccia exhibit both intrabasinal and



extrabasinal sources and are considered to reflect episodic collapse of the outer (western) margin of the basin. At Black Hill and north of the Dundas River (Fig. 1), significant thicknesses (> 400 m) of deformed *Cycle A* sediments occur intercalated with polymict conglomerate and mudstone-dominated turbidites. The former are interpreted as having been emplaced as westerly directed slide sheets during the deposition of *Cycle B*.

***Cycle C* (Late C):**

The appearance of white mica as a significant detrital component is interpreted as indicating the start of *Cycle C*. This feature, in association with the occurrence of oligomict conglomerate rich in orthoquartzite and quart-mica schist higher in the succession, indicates the emergence of the Tyennan Nucleus. This cycle of deposition therefore reflects the transition from reworking of intrabasinal sources to significant uplift and erosion of the basin margin. The basin-closing episode which initiated in the late Middle Cambrian (at the latest) is therefore considered to have continued (and possibly intensified) during the Late Cambrian.

## Reference

Crawford A. J. & Berry R. F., 1992. Tectonic implications of Late Proterozoic-Early Palaeozoic igneous rock associations in western Tasmania. Tectonophysics 214: 37-56.

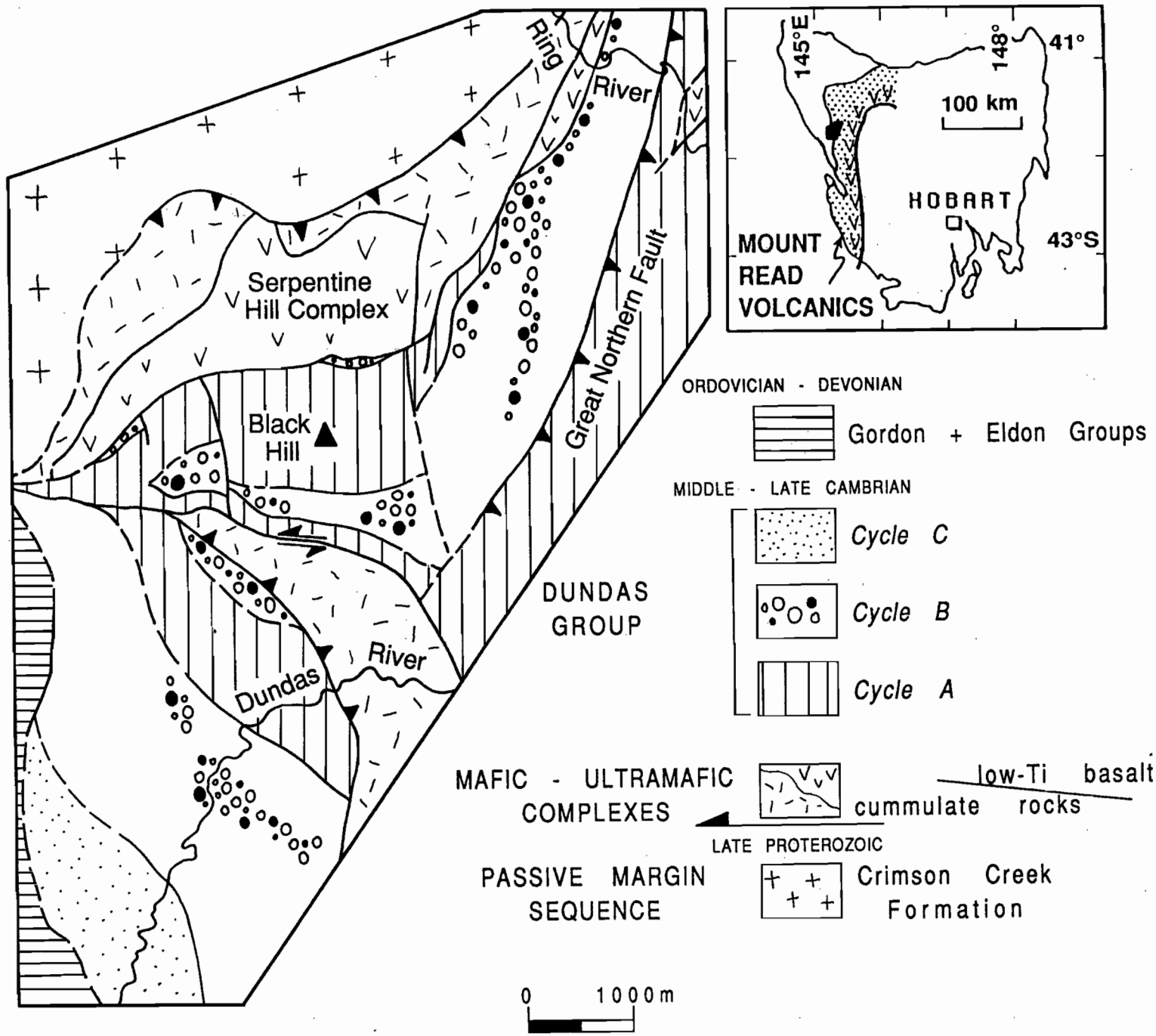


Figure 1. Simplified geological map of the Dundas River - Ring River district, showing distribution of depositional cycles.

Table 1. Depositional cycles of the Dundas Group and chrono-stratigraphic correlates. Note that "lithofacies" are arranged in no particular stratigraphic order.

| | LITHOFACIES | DUNDAS FORMATIONS | CHRONO - STRATIGRAPHIC CORRELATES | SOURCE | | | | EARLY STRUCTURES | FOSSIL AGES |
|---|---|---|---|---|---|---|---|---|---|
| | | | | ACTIVE MT READ VOLCANIC ARC | INTRABASINAL REWORKING | BASEMENT: PASSIVE MARGIN | BASEMENT: ALLOCHTHON | | |
| **CYCLE A** | • black shale<br>• pumiceous mass-flow deposits<br>• oligomict, framework-supported conglomerate / sandstone<br>• mudstone-dominated thinly bedded turbidites<br>• feldspar-phyric crystal rich sandstone | Hodge Slate<br>Razorback Congl.<br>Lower Brewery Junction Fm.<br>— | Que River Shale<br>White Spur Formation<br>Southwell Subgroup<br>Stitt Quartzite<br>Farrell Rivulet Congl.<br>Hatfield River beds<br>Sticht Range Beds<br>Comstock Tuff<br>Natone Volcanics | ● | ○ | ● | | • slides<br>• recumbent isoclinal folds<br>• zones of liquification | mid. Middle Ꞓ<br>↓<br>late Middle Ꞓ |
| **CYCLE B** | • mudstone-dominated thinly bedded turbidites<br>• polymict framework-supported conglomerate / sandstone<br>• mass-failure deposits: ( debris flows / talus breccias ) | Upper Brewery Jnc.<br>Comet Slate<br>Red Lead Congl.<br>Fernfields Congl.<br>Fernflow Congl. | Mt Cripps Subgroup<br>Upper Tyndall Group<br>Salisbury Congl. | | ● | ?○ | ○ | • slides<br>• gravitational collapse folds<br>• zones of liquification | late Middle Ꞓ<br>↓<br>early Late Ꞓ |
| **CYCLE C** | • micaceous silty mudstone<br>• polymict to oligomict framework-supported conglomerate | Climie Slate<br>Misery Hill Congl. | Owen Conglomerate<br>Higgins Creek beds | | ○ | ● | | • slides<br>• zones of liquification | Late Ꞓ |

● dominant source

○ subordinate source